

# Perturbative Corrections to $\Lambda_b \rightarrow \Lambda$ Form Factors from QCD Light-Cone Sum Rules

Yu-Ming Wang<sup>a,b</sup> and Yue-Long Shen<sup>c</sup>

<sup>a</sup> *Fakultät für Physik, Universität Wien, Boltzmanngasse 5, 1090 Vienna, Austria*

<sup>b</sup> *Physik Department T31, Technische Universität München, James-Franck-Straße 1, D-85748 Garching, Germany*

<sup>c</sup> *College of Information Science and Engineering, Ocean University of China, Qingdao, Shandong 266100, P.R. China*

## Abstract

We compute radiative corrections to  $\Lambda_b \rightarrow \Lambda$  form factors, at next-to-leading logarithmic accuracy, from QCD light-cone sum rules with  $\Lambda_b$ -baryon distribution amplitudes. Employing the diagrammatic approach factorization of the vacuum-to- $\Lambda_b$ -baryon correlation function is justified at leading power in  $\Lambda/m_b$ , with the aid of the method of regions. Hard functions entering the factorization formulae are identical to the corresponding matching coefficients of heavy-to-light currents from QCD onto soft-collinear effective theory. The universal jet function from integrating out the hard-collinear fluctuations exhibits richer structures compared with the one involved in the factorization expressions of the vacuum-to- $B$ -meson correlation function. Based upon the QCD resummation improved sum rules we observe that the perturbative corrections at  $\mathcal{O}(\alpha_s)$  shift the  $\Lambda_b \rightarrow \Lambda$  form factors at large recoil significantly and the dominant contribution originates from the next-to-leading order jet function instead of the hard coefficient functions. Having at hand the sum rule predictions for the  $\Lambda_b \rightarrow \Lambda$  form factors we further investigate several decay observables in the electro-weak penguin  $\Lambda_b \rightarrow \Lambda \ell^+ \ell^-$  transitions in the factorization limit (i.e., ignoring the “non-factorizable” hadronic effects which cannot be expressed in terms of the  $\Lambda_b \rightarrow \Lambda$  form factors), including the invariant mass distribution of the lepton pair, the forward-backward asymmetry in the dilepton system and the longitudinal polarization fraction of the leptonic sector.

# 1 Introduction

Electro-weak penguin  $b \rightarrow s\ell\ell$  decays are widely believed to be sensitive probes to physics beyond the Standard Model (SM) and continuous efforts have been devoted to investigations of exclusive  $B \rightarrow K^{(*)}\ell^+\ell^-$  decays towards understanding the strong interaction dynamics in QCD and constructing the optimized angular observables of phenomenological interest. Unfortunately, no evident new physics signals have been revealed in the exclusive  $B$ -meson decays yet, albeit with several “anomalies” under extensive discussions and debates. It is therefore natural to explore the dynamics of flavour-changing neutral current induced hadronic transitions in a complementary way.

In this respect the baryonic counter channels  $\Lambda_b \rightarrow \Lambda \ell^+\ell^-$  can serve the purpose thanks to the dedicated  $b$ -physics program at the LHC. Theory descriptions of exclusive heavy baryon decays have been initiated in the early days of the heavy-quark effective theory (HQET) in an attempt to understand the QCD dynamics of heavy quark decays, and they have attracted renewed attentions recently [1–3] towards a better understanding of the heavy-to-light baryonic form factors at large recoil in the heavy quark limit. Also, there are good arguments in favor of studying the exclusive  $\Lambda_b \rightarrow \Lambda \ell^+\ell^-$  decays on the phenomenological side. First, the polarization asymmetry of the  $\Lambda$ -baryon in the decay products allows a “clean” extraction of the helicity structure of the weak effective Hamiltonian in the factorization limit [4, 5]. Second, the angular distribution for the four-body decays  $\Lambda_b \rightarrow \Lambda(\rightarrow N\pi)\ell^+\ell^-$  offers additional information on the Wilson coefficients of effective weak operators [6], due to the fact that the cascade weak decay  $\Lambda \rightarrow N\pi$  is parity violating. Third, the systematic uncertainty entering the computation of the  $\Lambda_b \rightarrow \Lambda \ell^+\ell^-$  amplitude, induced by the  $\Lambda$ -baryon decay width, is negligible compared with the counterpart  $B \rightarrow K^*\ell^+\ell^-$  channels.

Precision QCD calculations of the electro-weak penguin decays  $\Lambda_b \rightarrow \Lambda \ell^+\ell^-$  are complicated by the poorly known hadronic form factors and by the notoriously “non-factorizable” hadronic effects defined by the non-local matrix elements of the weak operators acting together with the QED quark currents. The main purpose of this paper is to perform a complete analysis of 10 independent  $\Lambda_b \rightarrow \Lambda$  form factors, at  $\mathcal{O}(\alpha_s)$ , from QCD light-cone sum rules (LCSR) with the  $\Lambda_b$ -baryon distribution amplitudes (DA) originally developed in the context of the  $B$ -meson decays [7–10], paving the way for the construction of a systematic approach to the exclusive  $\Lambda_b \rightarrow \Lambda \ell^+\ell^-$  decays in analogy to the mesonic counterpart case [11]. As already emphasized in [12] one of the primary tasks of constructing the  $\Lambda_b$ -baryon LCSR is to demonstrate QCD factorization for the vacuum-to- $\Lambda_b$ -baryon correlation function in the proper kinematic regime. In the framework of soft-collinear effective theory (SCET) factorization of the correlation function defined with the “A-type” weak current and an interpolating current of the  $\Lambda$ -baryon was established at tree level in the heavy quark limit [2]. Instead of using the SCET technique we will, following [12], adopt the method of regions [13] to prove factorization of the vacuum-to- $\Lambda_b$ -baryon correlation function at next-to-leading-order (NLO) in  $\alpha_s$  diagrammatically and resum large logarithms in the short distance functions with the renormalization-group (RG) approach in momentum space.

Soft QCD dynamics of the vacuum-to- $\Lambda_b$ -baryon correlation function is parameterized by the non-perturbative but universal wave functions of the  $\Lambda_b$ -baryon [14] which also serves as fundamental inputs for the theory description of semileptonic  $\Lambda_b \rightarrow p\ell\nu$  transitions [15],

$\Lambda_b \rightarrow \Lambda_c \ell \nu$  decays [16] and hadronic  $\Lambda_b \rightarrow p \pi, p K$  decays [17]. Despite the recent progress in understanding the renormalization property of the twist-2  $\Lambda_b$ -baryon DA [18, 19], modelling the higher twist DA in compatible with the perturbative QCD constraints still demands dedicated studies. As we will observe later, it is actually the twist-4 DA of the  $\Lambda_b$ -baryon entering the QCD factorization formulae of the vacuum-to- $\Lambda_b$ -baryon correction functions, whose RG evolution equation at one loop is not explicitly known yet (though building blocks of the renormalization kernels for the desired light ray operators can be found in [20]). Investigating renormalization scale evolution of the convolution integral of the NLO twist-4 partonic DA and the tree-level hard kernel constitutes another non-trivial target of this paper.

Different QCD-based approaches were adopted in the literature to compute the  $\Lambda_b \rightarrow \Lambda$  form factors in addition to the recent Lattice QCD determinations [21]. A closely related approach was applied to construct the LCSR for  $\Lambda_b \rightarrow \Lambda$  form factors at tree level from the vacuum-to- $\Lambda$ -baryon correlation function [22] where the  $\Lambda$ -baryon DA entering the sum rules were only considered at the leading conformal spin accuracy (the non-asymptotic corrections were worked out in [23] now) and the Chernyak-Zhitnitsky [24] type of the  $\Lambda$ -baryon interpolating current was used (see [25, 26] for alternative choices and [27] for interesting comments on the choices of the baryonic interpolating currents). Another approach to compute the  $\Lambda_b \rightarrow \Lambda$  form factors based upon the transverse-momentum-dependent (TMD) factorization was carried out in [28] where the soft overlap contribution was assumed to be suppressed by the Sudakov factor and only the hard spectator interactions induced by two-hard-collinear-gluon exchanges are taken into account. A comparison of the resulting form factors from two different methods tends to indicate that the heavy-to-light baryonic form factors at large recoil is dominated by the *formally sub-leading* soft gluon exchanges instead of the leading power hard spectator contributions <sup>1</sup>.

The paper is organized as follows. In section 2 we first set up convention of the helicity-based parametrization of the  $\Lambda_b \rightarrow \Lambda$  form factors and then discuss the choice of the interpolating currents for the  $\Lambda$ -baryon and introduce the correlation functions for constructions of the LCSR for all the independent form factors. We also present the essential ingredients for proof of QCD factorization of the correlation functions and derive the tree level LCSR for  $\Lambda_b \rightarrow \Lambda$  form factors. Applying the method of regions we compute the hard coefficients and the jet functions at  $\mathcal{O}(\alpha_s)$  entering the QCD factorization formulae in section 3 where we demonstrate explicitly cancellation of the factorization-scale dependence in the correlation functions and resummation of large logarithms in the short-distance functions is also achieved at next-to-leading-logarithmic (NLL) accuracy with the standard RG approach. Resummation improved LCSR for the  $\Lambda_b \rightarrow \Lambda$  form factors presented in section 4 constitute the main new results of this paper. The details of the numerical analysis of the newly derived LCSR, including various sources of perturbative and systematic uncertainties, the  $z$ -series expansion and a comparison with the Lattice determinations at small recoil, are collected in section 5. Phenomenological applications of our results to the exclusive electro-weak penguin decays  $\Lambda_b \rightarrow \Lambda \ell^+ \ell^-$  at large recoil are discussed in the factorization limit in section 6. Section 7 is reserved for the concluding discussion. Appendix A contains dispersion representations of the

---

<sup>1</sup>Strictly speaking, separation of the soft overlap contributions (Feynman mechanism) and the hard-scattering effects are both factorization scale- and scheme- dependent.

convolution integrals entering expressions of the factorized correlation functions, which are essential to construct the LCSR for the  $\Lambda_b \rightarrow \Lambda$  form factors presented in section 4.

## 2 Tree-level LCSR of $\Lambda_b \rightarrow \Lambda$ form factors

### 2.1 Helicity-based $\Lambda_b \rightarrow \Lambda$ form factors

Following [2] we define  $\Lambda_b \rightarrow \Lambda$  form factors in the helicity basis which lead to rather compact expressions for angular distributions, unitary bounds and sum rules, and we collect the definitions as follows

$$\begin{aligned} \langle \Lambda(p', s') | \bar{s} \gamma_\mu b | \Lambda_b(p, s) \rangle &= \bar{\Lambda}(p', s') \left[ f_{\Lambda_b \rightarrow \Lambda}^0(q^2) \frac{m_{\Lambda_b} - m_\Lambda}{q^2} q_\mu \right. \\ &\quad + f_{\Lambda_b \rightarrow \Lambda}^+(q^2) \frac{m_{\Lambda_b} + m_\Lambda}{s_+} \left( (p + p')_\mu - \frac{m_{\Lambda_b}^2 - m_\Lambda^2}{q^2} q_\mu \right) \\ &\quad \left. + f_{\Lambda_b \rightarrow \Lambda}^T(q^2) \left( \gamma_\mu - \frac{2m_\Lambda}{s_+} p_\mu - \frac{2m_{\Lambda_b}}{s_+} p'_\mu \right) \right] \Lambda_b(p, s), \end{aligned} \quad (1)$$

$$\begin{aligned} \langle \Lambda(p', s') | \bar{s} \gamma_\mu \gamma_5 b | \Lambda_b(p, s) \rangle &= -\bar{\Lambda}(p', s') \gamma_5 \left[ g_{\Lambda_b \rightarrow \Lambda}^0(q^2) \frac{m_{\Lambda_b} + m_\Lambda}{q^2} q_\mu \right. \\ &\quad + g_{\Lambda_b \rightarrow \Lambda}^+(q^2) \frac{m_{\Lambda_b} - m_\Lambda}{s_-} \left( (p + p')_\mu - \frac{m_{\Lambda_b}^2 - m_\Lambda^2}{q^2} q_\mu \right) \\ &\quad \left. + g_{\Lambda_b \rightarrow \Lambda}^T(q^2) \left( \gamma_\mu + \frac{2m_\Lambda}{s_-} p_\mu - \frac{2m_{\Lambda_b}}{s_-} p'_\mu \right) \right] \Lambda_b(p, s), \end{aligned} \quad (2)$$

$$\begin{aligned} \langle \Lambda(p', s') | \bar{s} i \sigma_{\mu\nu} q^\nu b | \Lambda_b(p, s) \rangle &= -\bar{\Lambda}(p', s') \left[ h_{\Lambda_b \rightarrow \Lambda}^+(q^2) \frac{q^2}{s_+} \left( (p + p')_\mu - \frac{m_{\Lambda_b}^2 - m_\Lambda^2}{q^2} q_\mu \right) \right. \\ &\quad \left. + (m_{\Lambda_b} + m_\Lambda) h_{\Lambda_b \rightarrow \Lambda}^T(q^2) \left( \gamma_\mu - \frac{2m_\Lambda}{s_+} p_\mu - \frac{2m_{\Lambda_b}}{s_+} p'_\mu \right) \right] \Lambda_b(p, s), \end{aligned} \quad (3)$$

$$\begin{aligned} \langle \Lambda(p', s') | \bar{s} i \sigma_{\mu\nu} q^\nu \gamma_5 b | \Lambda_b(p, s) \rangle &= -\bar{\Lambda}(p', s') \gamma_5 \left[ \tilde{h}_{\Lambda_b \rightarrow \Lambda}^+(q^2) \frac{q^2}{s_-} \left( (p + p')_\mu - \frac{m_{\Lambda_b}^2 - m_\Lambda^2}{q^2} q_\mu \right) \right. \\ &\quad \left. + (m_{\Lambda_b} - m_\Lambda) \tilde{h}_{\Lambda_b \rightarrow \Lambda}^T(q^2) \left( \gamma_\mu + \frac{2m_\Lambda}{s_-} p_\mu - \frac{2m_{\Lambda_b}}{s_-} p'_\mu \right) \right] \Lambda_b(p, s), \end{aligned} \quad (4)$$

where  $m_{\Lambda_b}(s)$  is the mass (spin) of the  $\Lambda_b$ -baryon,  $m_\Lambda(s')$  is the mass (spin) of the  $\Lambda$ -baryon and we introduce

$$s_\pm = (m_{\Lambda_b} \pm m_\Lambda)^2 - q^2. \quad (5)$$

We work in the rest frame of the  $\Lambda_b$ -baryon with the velocity vector  $v_\mu = p_\mu/m_{\Lambda_b}$  and define a light-cone vector  $\bar{n}_\mu$  parallel to the four-momentum  $p'$  of the  $\Lambda$ -baryon in the massless limit.

Another light-cone vector can be introduced as  $n_\mu = 2v_\mu - \bar{n}_\mu$  with  $n \cdot \bar{n} = 2$  for the later convenience. At large hadronic recoil we write

$$n \cdot p' \simeq \frac{m_{\Lambda_b}^2 + m_\Lambda^2 - q^2}{m_{\Lambda_b}} = 2E_\Lambda \sim \mathcal{O}(m_{\Lambda_b}). \quad (6)$$

Exploiting the heavy quark symmetry and the collinear equations of motion yields [1, 2]

$$\begin{aligned} f_{\Lambda_b \rightarrow \Lambda}^0(q^2) &\simeq f_{\Lambda_b \rightarrow \Lambda}^+(q^2) \simeq f_{\Lambda_b \rightarrow \Lambda}^T(q^2) \simeq h_{\Lambda_b \rightarrow \Lambda}^+(q^2) \simeq h_{\Lambda_b \rightarrow \Lambda}^T(q^2) \\ &\simeq g_{\Lambda_b \rightarrow \Lambda}^0(q^2) \simeq g_{\Lambda_b \rightarrow \Lambda}^+(q^2) \simeq g_{\Lambda_b \rightarrow \Lambda}^T(q^2) \simeq \tilde{h}_{\Lambda_b \rightarrow \Lambda}^+(q^2) \simeq \tilde{h}_{\Lambda_b \rightarrow \Lambda}^T(q^2) \end{aligned} \quad (7)$$

at large recoil, where the strong interaction dynamics of the hadronic transitions is assumed to be dominated by the soft gluon exchanges. Hard spectator interactions induced by the two-hard-collinear-gluon exchanges are shown to still respect these symmetry relations at leading power in  $\Lambda/m_b$  [3], where  $\Lambda$  is a hadronic scale of order  $\Lambda_{\text{QCD}}$ . We will first confirm such form factor relations from the tree-level LCSR (see also [2]) and then compute the symmetry-breaking effects induced by the hard fluctuations of QCD decay currents (also known as the matching coefficients of weak currents from QCD onto SCET) and the one-loop jet function in the next section.

## 2.2 Interpolating currents and correlation function

Following the standard strategy we start with construction of the correlation function

$$\Pi_{\mu,a}(p, q) = i \int d^4x e^{iq \cdot x} \langle 0 | T \{ j_\Lambda(x), j_{\mu,a}(0) \} | \Lambda_b(p) \rangle, \quad (8)$$

where the local current  $j_\Lambda$  interpolates the  $\Lambda$ -baryon and  $j_{\mu,a}$  stands for the weak transition current  $\bar{s} \Gamma_{\mu,a} b$  with the index “ $a$ ” indicating a certain Lorenz structure, i.e.,

$$\begin{aligned} j_{\mu,V} &= \bar{s} \gamma_\mu b, & j_{\mu,A} &= \bar{s} \gamma_\mu \gamma_5 b, \\ j_{\mu,T} &= \bar{s} \sigma_{\mu\nu} q^\nu b, & j_{\mu,\tilde{T}} &= \bar{s} \sigma_{\mu\nu} q^\nu \gamma_5 b. \end{aligned} \quad (9)$$

As discussed in [29] the general structure of the  $\Lambda$ -baryon current reads

$$j_\Lambda = \epsilon_{ijk} (u_i^T C \Gamma d_j) \tilde{\Gamma} s_k, \quad (10)$$

where  $C$  is the charge conjugation matrix and the sum runs over the color indices  $i, j, k$ . Implementing the isospin constraint of the light diquark  $[ud]$  system we are left with three independent choices

$$j_\Lambda^A = \epsilon_{ijk} (u_i^T C \gamma_5 \not{n} d_j) s_k, \quad j_\Lambda^P = \epsilon_{ijk} (u_i^T C \gamma_5 d_j) s_k, \quad j_\Lambda^S = \epsilon_{ijk} (u_i^T C d_j) \gamma_5 s_k. \quad (11)$$

Projecting out the large and small components of the (hard)-collinear quark fields one can readily identify that the two currents  $j_\Lambda^P$  and  $j_\Lambda^S$  are power suppressed compared with the

axial-vector current  $j_\Lambda^A$ . Having in mind that the interpolating current should couple strongly to the  $\Lambda$ -baryon in order to minimize the contamination generated by its coupling to the unwanted hadronic states, we will only consider the axial-vector current  $j_\Lambda^A$  for construction of the correlation function.

To derive the hadronic dispersion relation of the correlation function we need to define the coupling of the  $\Lambda$ -baryon with the  $j_\Lambda^A$  current

$$\langle 0 | j_\Lambda^A | \Lambda(p') \rangle = f_\Lambda(\mu) (n \cdot p') \Lambda(p'), \quad (12)$$

where the renormalization scale dependence of  $f_\Lambda(\mu)$  is indicated explicitly and the corresponding evolution equation is given by

$$\frac{d}{d \ln \mu} \ln f_\Lambda(\mu) = - \left( \frac{\alpha_s(\mu)}{4\pi} \right)^k \gamma_\Lambda^{(k)}, \quad (13)$$

with  $\gamma_\Lambda^{(1)} = 4/3$  [30, 31]. It is then a straightforward task to write down the hadronic representations for the correlation functions defined with various weak currents

$$\begin{aligned} \Pi_{\mu,V}(p, q) &= \frac{f_\Lambda(\mu) (n \cdot p')}{m_\Lambda^2/n \cdot p' - \bar{n} \cdot p' - i0} \frac{\not{n}}{2} \left[ f_{\Lambda_b \rightarrow \Lambda}^T(q^2) \gamma_{\perp\mu} + \frac{f_{\Lambda_b \rightarrow \Lambda}^0(q^2) - f_{\Lambda_b \rightarrow \Lambda}^+(q^2)}{2(1 - n \cdot p'/m_{\Lambda_b})} n_\mu \right. \\ &\quad \left. + \frac{f_{\Lambda_b \rightarrow \Lambda}^0(q^2) + f_{\Lambda_b \rightarrow \Lambda}^+(q^2)}{2} \bar{n}_\mu \right] \Lambda_b(p) + \int_{\omega_s}^{+\infty} d\omega' \frac{1}{\omega' - \bar{n} \cdot p' - i0} \\ &\quad \times \frac{\not{n}}{2} \left[ \rho_{V,\perp}^h(\omega', n \cdot p') \gamma_{\perp\mu} + \rho_{V,n}^h(\omega', n \cdot p') n_\mu + \rho_{V,\bar{n}}^h(\omega', n \cdot p') \bar{n}_\mu \right] \Lambda_b(p), \end{aligned} \quad (14)$$

$$\begin{aligned} \Pi_{\mu,A}(p, q) &= \frac{f_\Lambda(\mu) (n \cdot p')}{m_\Lambda^2/n \cdot p' - \bar{n} \cdot p' - i0} \gamma_5 \frac{\not{n}}{2} \left[ g_{\Lambda_b \rightarrow \Lambda}^T(q^2) \gamma_{\perp\mu} + \frac{g_{\Lambda_b \rightarrow \Lambda}^0(q^2) - g_{\Lambda_b \rightarrow \Lambda}^+(q^2)}{2(1 - n \cdot p'/m_{\Lambda_b})} n_\mu \right. \\ &\quad \left. + \frac{g_{\Lambda_b \rightarrow \Lambda}^0(q^2) + g_{\Lambda_b \rightarrow \Lambda}^+(q^2)}{2} \bar{n}_\mu \right] \Lambda_b(p) + \int_{\omega_s}^{+\infty} d\omega' \frac{1}{\omega' - \bar{n} \cdot p' - i0} \\ &\quad \times \gamma_5 \frac{\not{n}}{2} \left[ \rho_{A,\perp}^h(\omega', n \cdot p') \gamma_{\perp\mu} + \rho_{A,n}^h(\omega', n \cdot p') n_\mu + \rho_{A,\bar{n}}^h(\omega', n \cdot p') \bar{n}_\mu \right] \Lambda_b(p), \end{aligned} \quad (15)$$

$$\begin{aligned} \Pi_{\mu,T}(p, q) &= -\frac{m_{\Lambda_b} f_\Lambda(\mu) (n \cdot p')}{m_\Lambda^2/n \cdot p' - \bar{n} \cdot p' - i0} \frac{\not{n}}{2} \left[ h_{\Lambda_b \rightarrow \Lambda}^T(q^2) \gamma_{\perp\mu} \right. \\ &\quad \left. + \frac{h_{\Lambda_b \rightarrow \Lambda}^+(q^2)}{2} \left( \left( 1 - \frac{n \cdot p'}{m_{\Lambda_b}} \right) \bar{n}_\mu - n_\mu \right) \right] \Lambda_b(p) + \int_{\omega_s}^{+\infty} d\omega' \frac{1}{\omega' - \bar{n} \cdot p' - i0} \\ &\quad \times \frac{\not{n}}{2} \left[ \rho_{T,\perp}^h(\omega', n \cdot p') \gamma_{\perp\mu} + \rho_{T,+}^h(\omega', n \cdot p') \left( \left( 1 - \frac{n \cdot p'}{m_{\Lambda_b}} \right) \bar{n}_\mu - n_\mu \right) \right] \Lambda_b(p), \end{aligned} \quad (16)$$

$$\begin{aligned} \Pi_{\mu,\bar{T}}(p, q) &= \frac{m_{\Lambda_b} f_\Lambda(\mu) (n \cdot p')}{m_\Lambda^2/n \cdot p' - \bar{n} \cdot p' - i0} \gamma_5 \frac{\not{n}}{2} \left[ \tilde{h}_{\Lambda_b \rightarrow \Lambda}^T(q^2) \gamma_{\perp\mu} \right. \\ &\quad \left. + \frac{\tilde{h}_{\Lambda_b \rightarrow \Lambda}^+(q^2)}{2} \left( \left( 1 - \frac{n \cdot p'}{m_{\Lambda_b}} \right) \bar{n}_\mu - n_\mu \right) \right] \Lambda_b(p) + \int_{\omega_s}^{+\infty} d\omega' \frac{1}{\omega' - \bar{n} \cdot p' - i0} \end{aligned}$$

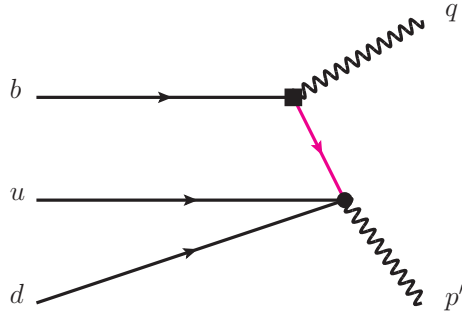


Figure 1: Diagrammatical representation of the correlation function  $\Pi_{\mu,a}(n \cdot p', \bar{n} \cdot p')$  at tree level, where the black square denotes the weak transition vertex, the black blob represents the Dirac structure of the  $\Lambda$ -baryon current and the pink internal line indicates the hard-collinear propagator of the strange quark.

$$\times \gamma_5 \frac{\not{n}}{2} \left[ \rho_{\bar{T},\perp}^h(\omega', n \cdot p') \gamma_{\perp\mu} + \rho_{\bar{T},+}^h(\omega', n \cdot p') \left( \left( 1 - \frac{n \cdot p'}{m_{\Lambda_b}} \right) \bar{n}_\mu - n_\mu \right) \right] \Lambda_b(p), \quad (17)$$

where we have defined

$$p' = p - q, \quad \gamma_{\perp\mu} = \gamma_\mu - \frac{\not{n}}{2} n_\mu - \frac{\not{n}}{2} \bar{n}_\mu. \quad (18)$$

Note also that we have naively assumed that effects from the negative-parity baryons with  $J^P = 1/2^-$  can be absorbed into the dispersion integrals in the above expressions and we refer to [29] for a detailed discussion of eliminating the “contamination” from such background contributions in the context of the LCSR with the nucleon DA.

### 2.3 Tree-level LCSR

Now we turn to compute the correlation function  $\Pi_{\mu,a}(p, q)$  at space-like interpolating momentum with  $|\bar{n} \cdot p'| \sim \mathcal{O}(\Lambda)$  and  $n \cdot p'$  fixed by Eq. (6), where light-cone operator-product-expansion (OPE) is applicable. Perturbative factorization of the partonic correlation function  $\Pi_{\mu,a}^{\text{par}}(p, q)$  (defined as replacing the hadronic state  $|\Lambda_b(p)\rangle$  by the on-shell partonic state  $|b(p_b)u(k_1)d(k_2)\rangle$  in Eq. (8)) at tree level takes the following form

$$\Pi_{\mu,a}^{\text{par}}(p, q) = \int d\omega'_1 \int d\omega'_2 T_{\alpha\beta\gamma\delta}^{(0)}(n \cdot p', \bar{n} \cdot p', \omega'_1, \omega'_2) \Phi_{bud}^{(0)\alpha\beta\delta}(\omega'_1, \omega'_2), \quad (19)$$

where the superscript (0) indicates the tree-level approximation and the Lorenz index “ $\mu$ ” is suppressed on the right-hand side in order not to overload the notation.

Evaluating the diagram in Fig. 1 leads to the leading-order hard kernel

$$T_{\alpha\beta\gamma\delta}^{(0)}(n \cdot p', \bar{n} \cdot p', \omega'_1, \omega'_2) = -\frac{1}{\bar{n} \cdot p' - \omega'_1 - \omega'_2 + i0} (C \gamma_5 \not{n})_{\alpha\beta} \left( \frac{\not{n}}{2} \Gamma_{\mu,a} \right)_{\gamma\delta}, \quad (20)$$

and the partonic DA of the  $\Lambda_b$ -baryon is defined as

$$\begin{aligned} \Phi_{bud}^{\alpha\beta\delta}(\omega'_1, \omega'_2) &= \int \frac{dt_1}{2\pi} \int \frac{dt_2}{2\pi} e^{i(\omega'_1 t_1 + \omega'_2 t_2)} \\ &\times \epsilon_{ijk} \langle 0 | [u_i^T(t_1 \bar{n})]_\alpha [0, t_1 \bar{n}] [d_j(t_2 \bar{n})]_\beta [0, t_2 \bar{n}] [b_k(0)]_\delta | b(v) u(k_1) d(k_2) \rangle, \end{aligned} \quad (21)$$

where the  $b$ -quark field needs to be understood as an effective heavy quark field in HQET and the light-cone Wilson line

$$[0, t \bar{n}] = P \left\{ \text{Exp} \left[ -i g_s t \int_0^1 du \bar{n} \cdot A(ut \bar{n}) \right] \right\} \quad (22)$$

is introduced with the convention of the covariant derivative in QCD as  $D_\mu = \partial_\mu - i g_s T^a A_\mu^a$ . The tree-level partonic DA entering the factorized expression (19) can be readily found to be

$$\Phi_{bud}^{(0)\alpha\beta\delta}(\omega'_1, \omega'_2) = \delta(\bar{n} \cdot k_1 - \omega'_1) \delta(\bar{n} \cdot k_2 - \omega'_2) \epsilon_{ijk} [u_i^T(k_1)]_\alpha [d_j(k_2)]_\beta [b_k(v)]_\delta. \quad (23)$$

Starting with the definition of the most-general light-cone hadronic matrix element in coordinate space [18]

$$\begin{aligned} \Phi_{\Lambda_b}^{\alpha\beta\delta}(t_1, t_2) &\equiv \epsilon_{ijk} \langle 0 | [u_i^T(t_1 \bar{n})]_\alpha [0, t_1 \bar{n}] [d_j(t_2 \bar{n})]_\beta [0, t_2 \bar{n}] [b_k(0)]_\delta | \Lambda_b(v) \rangle \\ &= \frac{1}{4} \left\{ f_{\Lambda_b}^{(1)}(\mu) \left[ \tilde{M}_1(v, t_1, t_2) \gamma_5 C^T \right]_{\beta\alpha} + f_{\Lambda_b}^{(2)}(\mu) \left[ \tilde{M}_2(v, t_1, t_2) \gamma_5 C^T \right]_{\beta\alpha} \right\} [\Lambda_b(v)]_\delta, \end{aligned} \quad (24)$$

performing the Fourier transformation and including the NLO terms off the light-cone leads to the momentum space light-cone projector in  $D$  dimensions

$$\begin{aligned} M_2(\omega'_1, \omega'_2) &= \frac{\not{n}}{2} \psi_2(\omega'_1, \omega'_2) + \frac{\not{n}}{2} \psi_4(\omega'_1, \omega'_2) \\ &\quad - \frac{1}{D-2} \gamma_\perp^\mu \left[ \psi_{\perp,1}^{+-}(\omega'_1, \omega'_2) \frac{\not{n}}{4} \frac{\not{n}}{\partial k_{1\perp}^\mu} + \psi_{\perp,1}^{-+}(\omega'_1, \omega'_2) \frac{\not{n}}{4} \frac{\not{n}}{\partial k_{1\perp}^\mu} \right] \\ &\quad - \frac{1}{D-2} \gamma_\perp^\mu \left[ \psi_{\perp,2}^{+-}(\omega'_2, \omega'_2) \frac{\not{n}}{4} \frac{\not{n}}{\partial k_{2\perp}^\mu} + \psi_{\perp,2}^{-+}(\omega'_1, \omega'_2) \frac{\not{n}}{4} \frac{\not{n}}{\partial k_{2\perp}^\mu} \right], \end{aligned} \quad (25)$$

$$\begin{aligned} M_1(\omega'_1, \omega'_2) &= \frac{\not{n}}{8} \psi_3^{+-}(\omega'_1, \omega'_2) + \frac{\not{n}}{8} \psi_3^{-+}(\omega'_1, \omega'_2) \\ &\quad - \frac{1}{D-2} \left[ \psi_{\perp,3}^{(1)}(\omega'_1, \omega'_2) \not{n} \gamma_\perp^\mu \frac{\partial}{\partial k_{1\perp}^\mu} + \psi_{\perp,3}^{(2)}(\omega'_1, \omega'_2) \gamma_\perp^\mu \not{n} \frac{\partial}{\partial k_{2\perp}^\mu} \right] \\ &\quad - \frac{1}{D-2} \left[ \psi_{\perp,Y}^{(1)}(\omega'_1, \omega'_2) \not{n} \gamma_\perp^\mu \frac{\partial}{\partial k_{1\perp}^\mu} + \psi_{\perp,Y}^{(2)}(\omega'_1, \omega'_2) \gamma_\perp^\mu \not{n} \frac{\partial}{\partial k_{2\perp}^\mu} \right], \end{aligned} \quad (26)$$

where we have adjusted the notation of the  $\Lambda_b$ -baryon DA defined in [18]. Applying the equations of motion in the Wandzura-Wilczek approximation [32] yields

$$\psi_{\perp,1}^{-+}(\omega'_1, \omega'_2) = \omega'_1 \psi_4(\omega'_1, \omega'_2), \quad \psi_{\perp,2}^{+-}(\omega'_1, \omega'_2) = \omega'_2 \psi_4(\omega'_1, \omega'_2). \quad (27)$$



It is now straightforward to derive the tree-level factorization formulae

$$\begin{aligned}
\Pi_{\mu,V(A)}^{(0)}(p,q) &= f_{\Lambda_b}^{(2)}(\mu) \int_0^{+\infty} d\omega'_1 \int_0^{+\infty} d\omega'_2 \frac{\psi_4(\omega'_1, \omega'_2)}{\omega'_1 + \omega'_2 - \bar{n} \cdot p' - i0} \\
&\quad \times (1, \gamma_5) \frac{\not{\bar{n}}}{2} (\gamma_{\perp\mu} + \bar{n}_\mu) \Lambda_b(v), \\
\Pi_{\mu,T(\bar{T})}^{(0)}(p,q) &= m_{\Lambda_b} f_{\Lambda_b}^{(2)}(\mu) \int_0^{+\infty} d\omega'_1 \int_0^{+\infty} d\omega'_2 \frac{\psi_4(\omega'_1, \omega'_2)}{\omega'_1 + \omega'_2 - \bar{n} \cdot p' - i0} \\
&\quad \times (-1, \gamma_5) \frac{\not{\bar{n}}}{2} \left[ \gamma_{\perp\mu} + \frac{1}{2} \left( \left( 1 - \frac{n \cdot p'}{m_{\Lambda_b}} \right) \bar{n}_\mu - n_\mu \right) \right] \Lambda_b(v), \tag{28}
\end{aligned}$$

at leading power in  $\Lambda/m_b$ . Employing the parton-hadronic duality approximation for the dispersion integrals in the hadronic representations and performing the continuum subtraction as well as the Borel transformation we obtain the tree-level LCSR

$$F_{\Lambda_b \rightarrow \Lambda}^i(q^2) = \frac{f_{\Lambda_b}^{(2)}(\mu)}{f_{\Lambda}(\mu) n \cdot p'} \exp \left[ \frac{m_{\Lambda}^2}{n \cdot p' \omega_M} \right] \int_0^{\omega_s} d\omega' e^{-\omega'/\omega_M} \tilde{\psi}_4(\omega') + \mathcal{O}(\alpha_s), \tag{29}$$

where  $F_{\Lambda_b \rightarrow \Lambda}^i(q^2)$  represents any of the 10  $\Lambda_b \rightarrow \Lambda$  form factors defined in section 2.1 and

$$\tilde{\psi}_4(\omega') = \omega' \int_0^1 du \psi_4(u\omega', (1-u)\omega'). \tag{30}$$

Applying the power counting scheme

$$\omega_s \sim \omega_M \sim \frac{\Lambda^2}{n \cdot p'}, \quad \tilde{\psi}_4(\omega') \sim \omega' \sim \omega_s, \tag{31}$$

the tree-level contribution (Feynman mechanism) to the  $\Lambda_b \rightarrow \Lambda$  form factors scales as  $1/(n \cdot p')^3$  in the large energy limit of the  $\Lambda$ -baryon, in agreement with the observations of [1, 2]. Since the large-recoil symmetry relations for the form factors are preserved at tree level, the symmetry violation effect, if it emerges at one loop, must be infrared finite due to the vanishing soft subtraction at  $\mathcal{O}(\alpha_s)$  in order not to invalidate QCD factorization of the correlation functions.

### 3 Factorization of the correlation function at $\mathcal{O}(\alpha_s)$

The purpose of this section is to compute the short-distance functions entering the factorization formulae of  $\Pi_{\mu,a}(p, q)$  at one loop

$$\Pi_{\mu,a}(p, q) = T \otimes \Phi_{bud} = C \cdot J \otimes \Phi_{bud}, \tag{32}$$

where  $\otimes$  denotes a convolution in the light-cone variables  $\omega'_1$  and  $\omega'_2$ . We will closely follow the strategies to prove the one-loop factorization of the vacuum-to- $B$ -meson correlation function detailed in [12] and employ the method of regions to evaluate the hard coefficients and the jet functions simultaneously. We further verify cancellation of the factorization-scale dependence of the correlation functions by computing convolution integrals of the NLO partonic DA and the tree-level hard kernel in (20) explicitly. Resummation of large logarithms involved in the perturbative functions is carried out at NLL using the momentum-space RG approach.

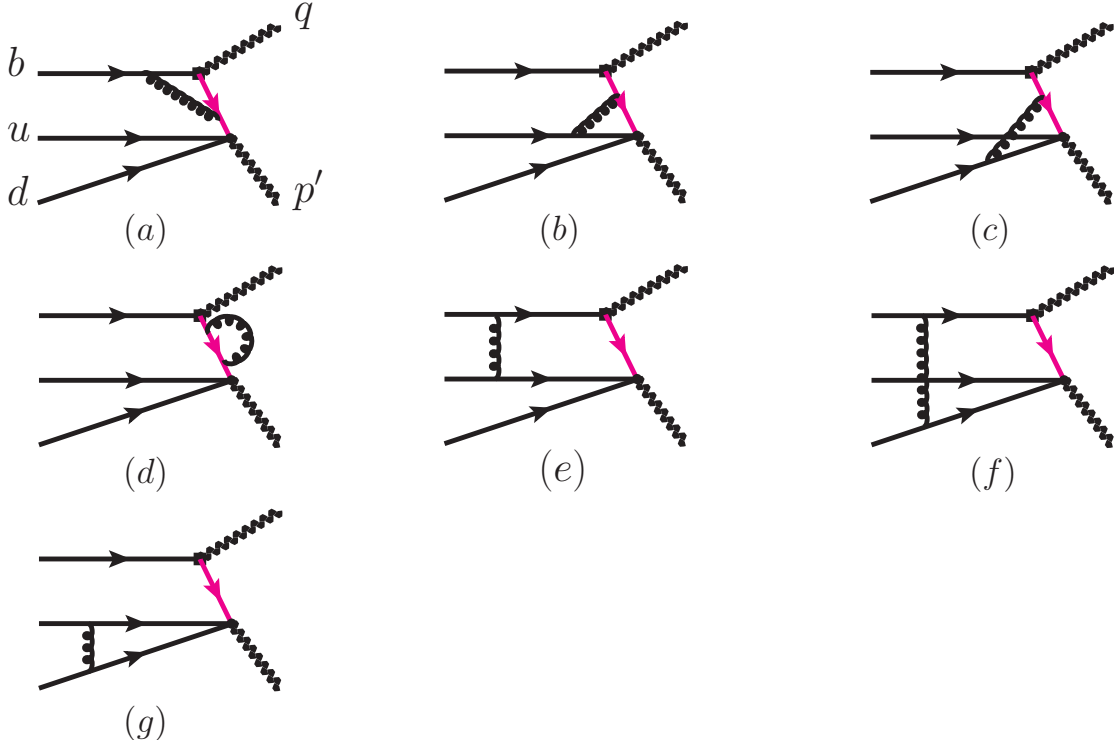


Figure 2: Diagrammatic representation of the correlation function  $\Pi_{\mu,a}(n \cdot p', \bar{n} \cdot p')$  at one loop. Same conventions as in Fig. 1.

### 3.1 Hard and jet functions at NLO

We are now ready to compute the one-loop QCD diagrams displayed in Fig. 2 for determinations of the perturbative matching coefficients. Since the loop integral entering the amplitude of the diagram (g) with one-gluon exchange between the two soft quarks does not contain any external hard and/or hard-collinear momentum modes, no contribution to the perturbative functions can arise from this diagram and we will compute the remaining diagrams one by one in the following. To facilitate the discussion of the one-loop calculation we will first focus on the (axial)-vector correlation functions  $\Pi_{\mu,V(A)}(p, q)$  and generalize the computation to the (pseudo)-tensor correlation functions  $\Pi_{\mu,T(\tilde{T})}(p, q)$  in the end of this section.

#### 3.1.1 Weak vertex diagram

Now we turn to compute the one-loop QCD correction to the weak vertex diagram displayed in Fig. 2(a)

$$\Pi_{\mu,V(A)}^{\text{par},a}(p, q) = \frac{i g_s^2 C_F}{\bar{n} \cdot p' - (\omega_1 + \omega_2) + i0} \int \frac{d^D l}{(2\pi)^D} \frac{1}{[(p' - k + l)^2 + i0][(m_b v + l)^2 - m_b^2 + i0][l^2 + i0]} \epsilon_{ijk} [u_i^T(k_1) C \gamma_5 \not{n} d_j(k_2)] \frac{\not{n}}{2} \gamma_\rho (\not{p}' - \not{k} + \not{l}) \gamma_\mu (1, \gamma_5) (m_b \not{p} + \not{l} + m_b) \gamma^\rho b_k(v), \quad (33)$$

where  $k = k_1 + k_2$ ,  $\omega_i = \bar{n} \cdot k_i$  ( $i = 1, 2$ ) and  $D = 4 - 2\epsilon$ . We have approximated the  $b$ -quark momentum as  $p_b = m_b v$  by dropping out the residual momentum, since we are only interested in extracting the leading power contributions to the correlation functions. The standard strategies to evaluate the perturbative matching coefficients would be: (i) first computing the loop integrals with the method of regions to determine the “bare” perturbative kernels without the ultraviolet (UV) and infrared (IR) subtractions, (ii) decomposing the resulting contributions in terms of independent operator bases (including the so-called “evanescent operators” [33, 34] whenever necessary) with the aid of the equations of motion, (iii) implementing the UV renormalization programs and infrared subtractions (determined by matrix elements of the effective operators), (iv) applying the momentum-space light-cone projector of the  $\Lambda_b$ -baryon to formulate factorized expressions of the correlation functions in the end. The above-mentioned procedures can be reduced in the absence of the “evanescent operators” as in our case, since no Fierz rearrangement is required in the perturbative matching:

$$i \int d^4x e^{iq \cdot x} T\{j_\Lambda(x), j_{\mu,a}(0)\} \rightarrow \sum_{i,j} \int dt_1 \int dt_2 \tilde{T}_{ij}(t_1, t_2, \bar{n} \cdot q, v \cdot q, m_b, \mu) [\Gamma_i]_{\alpha\beta} [\Gamma'_j]_{\gamma\delta} \\ \times \epsilon_{ijk} [u_i^T(t_1 \bar{n})]_\alpha [0, t_1 \bar{n}] [d_j(t_2 \bar{n})]_\beta [0, t_2 \bar{n}] [b_k(0)]_\delta . \quad (34)$$

The hard function contributed from Fig. 2(a) can be determined by expanding Eq. (33) in the hard region and by applying the light-cone projector subsequently and this leads to

$$\Pi_{\mu,V(A)}^{a,h}(p, q) \\ = i g_s^2 C_F \frac{f_{\Lambda_b}^{(2)}(\mu) \psi_4(\omega_1, \omega_2)}{\bar{n} \cdot p' - (\omega_1 + \omega_2) + i0} \int \frac{d^D l}{(2\pi)^D} \frac{1}{[(p' - k + l)^2 + i0][(m_b v + l)^2 - m_b^2 + i0][l^2 + i0]} \\ \times (1, \gamma_5) \frac{\not{n}}{2} \left\{ \gamma_{\perp\mu} \left[ n \cdot l ((D-2) \bar{n} \cdot l + 2m_b) + 2n \cdot p' (\bar{n} \cdot l + m_b) + (D-4) l_\perp^2 \right] \right. \\ \left. + n_\mu \left[ (2-D) (\bar{n} \cdot l)^2 \right] + \bar{n}_\mu \left[ 2m_b (n \cdot p' + n \cdot l) + (D-2) l_\perp^2 \right] \right\} \Lambda_b(v), \quad (35)$$

where the superscript “par” of the partonic correlation functions  $\Pi_{\mu,V(A)}^{a,h}$  is suppressed from now on and we have introduced

$$l_\perp^2 \equiv g_\perp^{\mu\nu} l_\mu l_\nu, \quad g_\perp^{\mu\nu} \equiv g^{\mu\nu} - \frac{n^\mu \bar{n}^\nu}{2} - \frac{n^\nu \bar{n}^\mu}{2}. \quad (36)$$

Evaluating the loop integrals with the formulae collected in Appendix A of [12] yields

$$\Pi_{\mu,V(A)}^{a,h}(p, q) = \frac{\alpha_s C_F}{4\pi} \frac{f_{\Lambda_b}^{(2)}(\mu) \psi_4(\omega_1, \omega_2)}{\bar{n} \cdot p' - (\omega_1 + \omega_2) + i0} (1, \gamma_5) \frac{\not{n}}{2} \\ \cdot \left[ \gamma_{\perp\mu} C_{h,\perp}^{(a)}(n \cdot p') + n_\mu C_{h,n}^{(a)}(n \cdot p') + \bar{n}_\mu C_{h,\bar{n}}^{(a)}(n \cdot p') \right], \quad (37)$$

where the coefficient functions read

$$C_{h,\perp}^{(a)}(n \cdot p') = \frac{1}{\epsilon^2} + \frac{1}{\epsilon} \left( 2 \ln \frac{\mu}{n \cdot p'} + 1 \right) + 2 \ln^2 \frac{\mu}{n \cdot p'} + 2 \ln \frac{\mu}{m_b} - 2 \text{Li}_2 \left( 1 - \frac{1}{r} \right)$$

$$-\ln^2 r + \frac{3r-2}{1-r} \ln r + \frac{\pi^2}{12} + 4, \quad (38)$$

$$C_{h,n}^{(a)}(n \cdot p') = \frac{1}{r-1} \left( 1 + \frac{r}{1-r} \ln r \right), \quad (39)$$

$$C_{h,\bar{n}}^{(a)}(n \cdot p') = \frac{1}{\epsilon^2} + \frac{1}{\epsilon} \left( 2 \ln \frac{\mu}{n \cdot p'} + 1 \right) + 2 \ln^2 \frac{\mu}{n \cdot p'} + 2 \ln \frac{\mu}{m_b} - 2 \text{Li}_2 \left( 1 - \frac{1}{r} \right) - \ln^2 r + \frac{2-r}{r-1} \ln r + \frac{\pi^2}{12} + 3, \quad (40)$$

with  $r = n \cdot p' / m_b$ .

By proceeding in a similar way, we can extract the hard-collinear contribution from Fig. 2(a) as follows

$$\begin{aligned} \Pi_{\mu,V(A)}^{a,hc}(p,q) &= i g_s^2 C_F \frac{f_{\Lambda_b}^{(2)}(\mu) \psi_4(\omega_1, \omega_2)}{\bar{n} \cdot p' - (\omega_1 + \omega_2) + i0} (1, \gamma_5) \frac{\not{n}}{2} [\gamma_{\perp\mu} + \bar{n}_\mu] \Lambda_b(v) \\ &\int \frac{d^D l}{(2\pi)^D} \frac{2 m_b n \cdot (p' + l)}{[n \cdot (p' + l) \bar{n} \cdot (p' - k + l) + l_\perp^2 + i0][m_b n \cdot l + i0][l^2 + i0]}, \end{aligned} \quad (41)$$

where the loop integrals are identical to the corresponding case in the vacuum-to- $B$ -meson correlation function [12]. We then write

$$\begin{aligned} \Pi_{\mu,V(A)}^{a,hc}(p,q) &= -\frac{\alpha_s C_F}{4\pi} \frac{f_{\Lambda_b}^{(2)}(\mu) \psi_4(\omega_1, \omega_2)}{\bar{n} \cdot p' - (\omega_1 + \omega_2) + i0} (1, \gamma_5) \frac{\not{n}}{2} [\gamma_{\perp\mu} + \bar{n}_\mu] \Lambda_b(v) \\ &\times \left[ \frac{2}{\epsilon^2} + \frac{2}{\epsilon} \left( \ln \frac{\mu^2}{n \cdot p' (\omega - \bar{n} \cdot p')} + 1 \right) + \ln^2 \frac{\mu^2}{n \cdot p' (\omega - \bar{n} \cdot p')} \right. \\ &\left. + 2 \ln \frac{\mu^2}{n \cdot p' (\omega - \bar{n} \cdot p')} - \frac{\pi^2}{6} + 4 \right], \end{aligned} \quad (42)$$

with  $\omega = \omega_1 + \omega_2$ .

To facilitate the determination of the jet function for the (pseudo)-tensor correlation functions  $\Pi_{\mu,T(\bar{T})}(p,q)$ , we can just expand Eq. (33) in the hard-collinear region without employing the light-cone projector in momentum space

$$\begin{aligned} \Pi_{\mu,V(A)}^{a,hc}(p,q) &= \frac{i g_s^2 C_F}{\bar{n} \cdot p' - (\omega_1 + \omega_2) + i0} \int \frac{d^D l}{(2\pi)^D} \\ &\frac{2 m_b n \cdot (p' + l)}{[n \cdot (p' + l) \bar{n} \cdot (p' - k + l) + l_\perp^2 + i0][m_b n \cdot l + i0][l^2 + i0]} \\ &\epsilon_{ijk} [u_i^\text{T}(k_1) C \gamma_5 \not{n} d_j(k_2)] \frac{\not{n}}{2} \gamma_\mu (1, \gamma_5) b_k(v), \end{aligned} \quad (43)$$

where no information of the weak vertex is used for reduction of the Dirac algebra. It is then evident that the hard-collinear contribution from Fig. 2(a) is *independent* of Lorenz structure of the weak vertex, at leading power in  $\Lambda/m_b$ .

### 3.1.2 $\Lambda$ -baryon vertex diagrams

The one-loop contributions to  $\Pi_{\mu,V(A)}(p, q)$  from the  $\Lambda$ -baryon vertex diagrams shown in Fig. 2(b) and 2(c) are given by

$$\begin{aligned} \Pi_{\mu,V(A)}^b(p, q) &= -\frac{i}{2} g_s^2 \left(1 + \frac{1}{N_c}\right) \frac{1}{n \cdot p' [\bar{n} \cdot p' - (\omega_1 + \omega_2) + i0]} \\ &\times \int \frac{d^D l}{(2\pi)^D} \frac{1}{[(p' - k_2 - l)^2 + i0][(l - k_1)^2 + i0][l^2 + i0]} \\ &\times \epsilon_{ijk} [u_i^T(k_1) C \gamma_\rho \not{l} \gamma_5 \not{k} d_j(k_2)] (\not{p}' - \not{k}_2 - \not{l}) \gamma^\rho (\not{p}' - \not{k}_1 - \not{k}_2) \gamma_\mu (1, \gamma_5) b_k(v), \end{aligned} \quad (44)$$

$$\Pi_{\mu,V(A)}^c(p, q) = \Pi_{\mu,V(A)}^b(p, q) [k_1 \leftrightarrow k_2], \quad (45)$$

where the isospin symmetry has been employed to derive the second equation. As already discussed in [12] it is more transparent to compute the loop integrals in Eq. (44) exactly instead of applying the method of regions, then keeping only the leading power terms in the resulting partonic amplitude and inserting the light-cone projector of the  $\Lambda_b$ -baryon. The three-point integral

$$\frac{(4\pi)^2}{i} \int \frac{d^D l}{(2\pi)^D} \frac{l_\alpha (p' - k_2 - l)_\beta}{[(p' - k_2 - l)^2 + i0][(l - k_1)^2 + i0][l^2 + i0]} \quad (46)$$

can be deduced from Eq. (120) of [12] with the following replacement rules

$$p \rightarrow p' - k_2, \quad k \rightarrow k_1. \quad (47)$$

Based upon the argument from the power counting analysis, the leading power contribution to  $\Pi_{\mu,V(A)}^b(p, q)$  can only arise from the hard-collinear region and the resulting contribution to the jet function is found to be

$$\begin{aligned} \Pi_{\mu,V(A)}^{b,hc}(p, q) &= -\frac{\alpha_s}{4\pi} \left(1 + \frac{1}{N_c}\right) \frac{f_{\Lambda_b}^{(2)}(\mu) \psi_4(\omega_1, \omega_2)}{\bar{n} \cdot p' - (\omega_1 + \omega_2) + i0} (1, \gamma_5) \frac{\not{n}}{2} [\gamma_{\perp\mu} + \bar{n}_\mu] \Lambda_b(v) \\ &\times \left\{ \left[ \frac{1 + \eta_2}{\eta_1} \ln \frac{1 + \eta_{12}}{1 + \eta_2} - \frac{3}{4} \right] \left[ \frac{1}{\epsilon} + \ln \frac{\mu^2}{n \cdot p' (\omega_2 - \bar{n} \cdot p')} - \frac{1}{2} \ln \frac{1 + \eta_{12}}{1 + \eta_2} \right. \right. \\ &\quad \left. \left. + \frac{5}{8} \frac{\eta_1}{1 + \eta_2} + 2 \right] + \frac{15}{32} \frac{\eta_1}{1 + \eta_2} - \frac{1}{4} \right\}, \end{aligned} \quad (48)$$

where we have defined

$$\eta_i = -\omega_i / \bar{n} \cdot p' \quad (i = 1, 2), \quad \eta_{12} = \eta_1 + \eta_2, \quad (49)$$

and the first relation in Eq. (27) due to the equations of motion have been implemented.

### 3.1.3 Wave function renormalization

The hard-collinear contribution from the self-energy correction to the intermediate quark propagator in Fig. 2(d) is independent of the Dirac structures of the weak transition current and the baryonic interpolating current. It is straightforward to write

$$\begin{aligned} \Pi_{\mu,V(A)}^{d,hc}(p, q) &= \frac{\alpha_s C_F}{4\pi} \frac{f_{\Lambda_b}^{(2)}(\mu) \psi_4(\omega_1, \omega_2)}{\bar{n} \cdot p' - (\omega_1 + \omega_2) + i0} (1, \gamma_5) \frac{\not{n}}{2} [\gamma_{\perp\mu} + \bar{n}_\mu] \Lambda_b(v) \\ &\times \left[ \frac{1}{\epsilon} + \ln \frac{\mu^2}{n \cdot p'(\omega - \bar{n} \cdot p')} + 1 \right]. \end{aligned} \quad (50)$$

The contributions of the wave function renormalization to the external quark fields can be taken from [12]

$$\begin{aligned} \Pi_{\mu,V(A)}^{bwf,(1)} - \Phi_{bud,bwf}^{(1)} \otimes T^{(0)} &= \frac{\alpha_s C_F}{8\pi} \frac{f_{\Lambda_b}^{(2)}(\mu) \psi_4(\omega_1, \omega_2)}{\bar{n} \cdot p' - (\omega_1 + \omega_2) + i0} (1, \gamma_5) \frac{\not{n}}{2} [\gamma_{\perp\mu} + \bar{n}_\mu] \Lambda_b(v) \\ &\times \left[ \frac{3}{\epsilon} + 3 \ln \frac{\mu^2}{m_b^2} + 4 \right], \end{aligned} \quad (51)$$

$$\Pi_{\mu,V(A)}^{uwf,(1)} - \Phi_{bud,uwf}^{(1)} \otimes T^{(0)} = \Pi_{\mu,V(A)}^{dwf,(1)} - \Phi_{bud,dwf}^{(1)} \otimes T^{(0)} = 0, \quad (52)$$

where  $\Pi_{\mu,V(A)}^{qwf,(1)}$  ( $q = b, u, d$ ) stands for the contribution to  $\Pi_{\mu,V(A)}$  from the wave function renormalization of the  $q$ -quark field at one loop, and  $\Phi_{bud,qwf}^{(1)}$  denotes the one-loop contribution to  $\Phi_{bud}$  defined in Eq. (21) from field renormalization of the  $q$ -quark.

### 3.1.4 Box diagrams

We proceed to compute the one-loop contributions from the two box diagrams displayed in Fig. 2(e) and 2(f). We can readily write

$$\begin{aligned} &\Pi_{\mu,V(A)}^e(p, q) \\ &= -\frac{i}{2} g_s^2 \left( 1 + \frac{1}{N_c} \right) \int \frac{d^D l}{(2\pi)^D} \frac{1}{[(p' - k + l)^2 + i0][(m_b v + l)^2 - m_b^2 + i0][(l - k_1)^2 + i0][l^2 + i0]} \\ &\quad \epsilon_{ijk} [u_i^T(k_1) C \gamma_\rho (k_1 - l) \gamma_5 \not{n} d_j(k_2)] (\not{p}' - k + l) \gamma_\mu (1, \gamma_5) (m_b \not{p} + l + m_b) \gamma^\rho b_k(v). \end{aligned} \quad (53)$$

With the isospin symmetry of exchanging the up and down quark fields we can again find

$$\Pi_{\mu,V(A)}^f(p, q) = \Pi_{\mu,V(A)}^e(p, q) [k_1 \leftrightarrow k_2]. \quad (54)$$

It is evident that no hard contribution can arise from the box diagrams and the contribution to the jet function from Fig. 2(e) can be determined by expanding Eq. (53) in the hard collinear region systematically

$$\Pi_{\mu,V(A)}^{e,hc}(p, q) = i g_s^2 \left( 1 + \frac{1}{N_c} \right) \int \frac{d^D l}{(2\pi)^D}$$

$$\frac{n \cdot (p' + l)}{[n \cdot (p' + l) \bar{n} \cdot (p' - k + l) + l_{\perp}^2 + i0][n \cdot l \bar{n} \cdot (l - k_1) + l_{\perp}^2 + i0][l^2 + i0]} \epsilon_{ijk} [u_i^T(k_1) C \gamma_5 \not{n} d_j(k_2)] \frac{\not{n}}{2} \gamma_{\mu} (1, \gamma_5) b_k(v). \quad (55)$$

We therefore conclude that the hard-collinear contribution induced by Fig. 2(e) is *independent* of the spin structure of the weak current, given the fact that only the Taylor expansion of the integrand in Eq. (53) at leading power in  $\Lambda/m_b$  and the equation of motion for the effective  $b$ -quark are needed in obtaining Eq. (55).

The loop integral entering the hard collinear contribution of Fig. 2(e) can be deduced from Eq. (128) of [12] with the substitution rules

$$n \cdot p \rightarrow n \cdot p', \quad \bar{n} \cdot p \rightarrow \bar{n} \cdot (p' - k_2), \quad \bar{n} \cdot k \rightarrow \bar{n} \cdot k_1. \quad (56)$$

Applying the momentum-space projector of the  $\Lambda_b$ -baryon we find

$$\begin{aligned} \Pi_{\mu, V(A)}^{e, hc}(p, q) &= \frac{\alpha_s}{4\pi} \left(1 + \frac{1}{N_c}\right) \frac{f_{\Lambda_b}^{(2)}(\mu) \psi_4(\omega_1, \omega_2)}{\bar{n} \cdot p' - (\omega_1 + \omega_2) + i0} (1, \gamma_5) \frac{\not{n}}{2} [\gamma_{\perp\mu} + \bar{n}_{\mu}] \Lambda_b(v) \\ &\times \left[ \frac{1 + \eta_{12}}{\eta_1} \ln \frac{1 + \eta_{12}}{1 + \eta_2} \right] \left[ \frac{1}{\epsilon} + \ln \frac{\mu^2}{n \cdot p' (\omega - \bar{n} \cdot p')} + \frac{1}{2} \ln \frac{1 + \eta_{12}}{1 + \eta_2} + 1 \right]. \quad (57) \end{aligned}$$

### 3.1.5 The NLO hard-scattering kernels

Now we are ready to determine the one-loop hard kernels entering QCD factorization formulae of the correlation functions  $\Pi_{\mu, V(A)}^{\text{par}}(p, q)$  by collecting different pieces together

$$\begin{aligned} \Phi_{bud}^{(0)} \otimes T_{V(A)}^{(1)} &= \left[ \Pi_{\mu, V(A)}^{a, h} + \left( \Pi_{\mu, V(A)}^{b, hf, (1)} - \Phi_{bud, b, hf}^{(1)} \otimes T^{(0)} \right) \right] \\ &+ \left[ \Pi_{\mu, V(A)}^{a, hc} + \Pi_{\mu, V(A)}^{b, hc} + \Pi_{\mu, V(A)}^{c, hc} + \Pi_{\mu, V(A)}^{d, hc} + \Pi_{\mu, V(A)}^{e, hc} + \Pi_{\mu, V(A)}^{f, hc} \right], \quad (58) \end{aligned}$$

where the terms in the first and second square brackets correspond to the hard and jet functions at  $\mathcal{O}(\alpha_s)$ , respectively. Introducing the definition

$$\Pi_{\mu, V(A)} = (1, \gamma_5) \frac{\not{n}}{2} \left[ \Pi_{\perp, V(A)} \gamma_{\perp\mu} + \Pi_{\bar{n}, V(A)} \bar{n}_{\mu} + \Pi_{n, V(A)} n_{\mu} \right] \Lambda_b(v), \quad (59)$$

we can readily obtain the following factorization formulae for the vacuum-to- $\Lambda_b$ -baryon correlation functions at NLO

$$\begin{aligned} \Pi_{\perp, V(A)} &= f_{\Lambda_b}^{(2)}(\mu) C_{\perp, V(A)}(n \cdot p', \mu) \int_0^{\infty} d\omega_1 \int_0^{\infty} d\omega_2 \frac{1}{\omega_1 + \omega_2 - \bar{n} \cdot p' - i0} \\ &J \left( \frac{\mu^2}{\bar{n} \cdot p' \omega_i}, \frac{\omega_i}{\bar{n} \cdot p'} \right) \psi_4(\omega_1, \omega_2, \mu), \quad (60) \end{aligned}$$

$$\begin{aligned} \Pi_{\bar{n},V(A)} &= f_{\Lambda_b}^{(2)}(\mu) C_{\bar{n},V(A)}(n \cdot p', \mu) \int_0^\infty d\omega_1 \int_0^\infty d\omega_2 \frac{1}{\omega_1 + \omega_2 - \bar{n} \cdot p' - i0} \\ &\quad J\left(\frac{\mu^2}{\bar{n} \cdot p' \omega_i}, \frac{\omega_i}{\bar{n} \cdot p'}\right) \psi_4(\omega_1, \omega_2, \mu), \end{aligned} \quad (61)$$

$$\Pi_{n,V(A)} = f_{\Lambda_b}^{(2)}(\mu) C_{n,V(A)}(n \cdot p', \mu) \int_0^\infty d\omega_1 \int_0^\infty d\omega_2 \frac{\psi_4(\omega_1, \omega_2, \mu)}{\omega_1 + \omega_2 - \bar{n} \cdot p' - i0}, \quad (62)$$

where the renormalized hard coefficients are given by

$$\begin{aligned} C_{\perp,V(A)}(n \cdot p', \mu) &= 1 - \frac{\alpha_s(\mu) C_F}{4\pi} \left[ 2 \ln^2 \frac{\mu}{n \cdot p'} + 5 \ln \frac{\mu}{m_b} - 2 \text{Li}_2\left(1 - \frac{1}{r}\right) \right. \\ &\quad \left. - \ln^2 r + \frac{3r-2}{1-r} \ln r + \frac{\pi^2}{12} + 6 \right], \end{aligned} \quad (63)$$

$$\begin{aligned} C_{\bar{n},V(A)}(n \cdot p', \mu) &= 1 - \frac{\alpha_s(\mu) C_F}{4\pi} \left[ 2 \ln^2 \frac{\mu}{n \cdot p'} + 5 \ln \frac{\mu}{m_b} - 2 \text{Li}_2\left(1 - \frac{1}{r}\right) \right. \\ &\quad \left. - \ln^2 r + \frac{2-r}{r-1} \ln r + \frac{\pi^2}{12} + 5 \right], \end{aligned} \quad (64)$$

$$C_{n,V(A)}(n \cdot p', \mu) = -\frac{\alpha_s(\mu) C_F}{4\pi} \left[ \frac{1}{r-1} \left( 1 + \frac{r}{1-r} \ln r \right) \right], \quad (65)$$

and the renormalized jet function reads

$$\begin{aligned} &J\left(\frac{\mu^2}{\bar{n} \cdot p' \omega_i}, \frac{\omega_i}{\bar{n} \cdot p'}\right) \\ &= 1 + \frac{\alpha_s(\mu)}{4\pi} \frac{4}{3} \left\{ \ln^2 \frac{\mu^2}{n \cdot p' (\omega - \bar{n} \cdot p')} - 2 \ln \frac{\omega - \bar{n} \cdot p'}{\omega_2 - \bar{n} \cdot p'} \ln \frac{\mu^2}{n \cdot p' (\omega - \bar{n} \cdot p')} \right. \\ &\quad \left. - \frac{1}{2} \ln \frac{\mu^2}{n \cdot p' (\omega - \bar{n} \cdot p')} - \ln^2 \frac{\omega - \bar{n} \cdot p'}{\omega_2 - \bar{n} \cdot p'} + 2 \ln \frac{\omega - \bar{n} \cdot p'}{\omega_2 - \bar{n} \cdot p'} \left[ \frac{\omega_2 - \bar{n} \cdot p'}{\omega_1} - \frac{3}{4} \right] \right. \\ &\quad \left. - \frac{\pi^2}{6} - \frac{1}{2} \right\}. \end{aligned} \quad (66)$$

Several comments on QCD factorization of the correlation functions  $\Pi_{\mu,V(A)}$  at NLO are in order.

- Since one universal jet function enters the factorization formulae of the correlation functions at  $\mathcal{O}(\alpha_s)$  and at leading power in  $\Lambda/m_b$ , the symmetry breaking effects of the form factor relations in Eq. (7) can only arise from the perturbative fluctuations at  $m_b$  scale, as reflected by the distinct hard functions for different weak currents. To determine the hard collinear contribution to the large-energy symmetry violations, we need to evaluate a *specific* sub-leading power contribution to the correlation functions induced by the  $\Lambda$ -baryon current. Technically, this can be achieved by introducing the



vacuum-to- $\Lambda_b$ -baryon correlation functions with the “wrong” light-cone projector acting on the  $\Lambda$ -baryon current as proposed in [2]. The hard-collinear symmetry breaking effects are shown to be of the same power in  $\Lambda/m_b$  as the soft overlap contributions, despite the fact that they are computed with the sum rules constructed from the power-suppressed correlation functions. This is by all means not surprising, because hadronic dispersion relations of the sub-leading correlation functions also involve an additional power-suppressed factor  $m_\Lambda/n \cdot p'$ . However, the numerical impacts of such hard-collinear symmetry violations defined by a hadronic matrix element of the “B-type” SCET current turn out to be insignificant from the same LCSR approach [2], we will therefore not include it in the following analysis. Also, evaluating hadronic matrix elements from the power-suppressed correlation functions are less favored from the standard philosophy of QCD sum rules, since the systematic uncertainty generated by the parton-hadron duality approximation is difficult to be under control.

- In naive dimension regularization the hard matching coefficients satisfy the relations  $C_{\perp,V} = C_{\perp,A}$ ,  $C_{\bar{n},V} = C_{\bar{n},A}$  and  $C_{n,V} = C_{n,A}$  to all orders in perturbation theory due to the U(1) helicity symmetry for both massless QCD and SCET Lagrangian functions [35]. It is then evident that the axial-vector  $\Lambda_b \rightarrow \Lambda$  form factors at large hadronic recoil will be identical to the corresponding vector form factors within our approximations.
- Only the weak vertex diagram and the two box diagrams could in principle yield hard-collinear contributions sensitive to the Dirac structure of the weak current, however, such sensitivity is shown to disappear at leading power in  $\Lambda/m_b$  after expanding the involved loop integrals in the hard-collinear region, as indicated by Eqs. (43) and (55). This leads us to conclude that the hard-collinear contributions to the correlation functions  $\Pi_{\mu,a}(p, q)$  are *independent* of the spin structure of the weak transition current, at leading power in  $\Lambda/m_b$ .

We now turn to consider factorization of the (pseudo)-tensor correlation functions  $\Pi_{\mu,T(\tilde{T})}$  at one loop. The hard coefficient functions can be extracted from the matching calculation of the weak (pseudo)-tensor currents from QCD onto SCET [36]

$$\begin{aligned}
& [\bar{q}(0) (1, \gamma_5) i \sigma_{\mu\nu} b(0)]_{\text{QCD}} \\
& \rightarrow \int d\hat{s} [\bar{\xi} W_{hc}] (s n) (1, \gamma_5) \left\{ \tilde{C}_{T(\tilde{T})}^A(\hat{s}) [i \sigma_{\mu\nu}] + \tilde{C}_{T(\tilde{T})}^B(\hat{s}) [\bar{n}_\mu \gamma_\nu - \bar{n}_\nu \gamma_\mu] \right\} [S^\dagger h](0) + \dots, \quad (67)
\end{aligned}$$

where the ellipses stand for the terms absent at  $\mathcal{O}(\alpha_s)$  as well as the sub-leading power currents, and we have defined the dimensionless convolution variable  $\hat{s} = s m_b$ . We have introduced the hard-collinear and the soft Wilson lines

$$\begin{aligned}
W_{hc}(x) &= \text{P} \left\{ \text{Exp} \left[ i g_s \int_{-\infty}^0 dt n \cdot A_{hc}(x + t n) \right] \right\}, \\
S(x) &= \text{P} \left\{ \text{Exp} \left[ i g_s \int_{-\infty}^0 dt \bar{n} \cdot A_s(x + t \bar{n}) \right] \right\} \quad (68)
\end{aligned}$$

to construct the building blocks invariant under both soft and hard-collinear gauge transformations. Performing the Fourier transformation from the momentum space to the position space yields [35, 36]

$$C_{T(\tilde{T})}^A(n \cdot p', \mu) = 1 - \frac{\alpha_s(\mu) C_F}{4\pi} \left[ 2 \ln^2 \frac{\mu}{n \cdot p'} + 7 \ln \frac{\mu}{m_b} - 2 \text{Li}_2 \left( 1 - \frac{1}{r} \right) - \ln^2 r + \frac{4r-2}{1-r} \ln r + \frac{\pi^2}{12} + 6 \right], \quad (69)$$

$$C_{T(\tilde{T})}^B(n \cdot p', \mu) = \frac{\alpha_s(\mu) C_F}{4\pi} \left[ \frac{2r}{1-r} \ln r \right]. \quad (70)$$

Decomposing the correlation functions  $\Pi_{\mu, T(\tilde{T})}$  in terms of Lorenz invariant amplitudes

$$\Pi_{\mu, T(\tilde{T})} = (-1, \gamma_5) \frac{\not{n}}{2} \left[ \Pi_{\perp, T(\tilde{T})} \gamma_{\perp\mu} + \frac{\Pi_{+, T(\tilde{T})}}{2} \left( \left( 1 - \frac{n \cdot p'}{m_{\Lambda_b}} \right) \bar{n}_\mu - n_\mu \right) \right] \Lambda_b(v), \quad (71)$$

it is straightforward to derive the factorization formulae

$$\begin{aligned} \Pi_{\perp, T(\tilde{T})} &= m_{\Lambda_b} f_{\Lambda_b}^{(2)}(\mu) C_{T(\tilde{T})}^A(n \cdot p', \mu) \int_0^\infty d\omega_1 \int_0^\infty d\omega_2 \frac{1}{\omega_1 + \omega_2 - \bar{n} \cdot p' - i0} \\ &\quad J \left( \frac{\mu^2}{\bar{n} \cdot p' \omega_i}, \frac{\omega_i}{\bar{n} \cdot p'} \right) \psi_4(\omega_1, \omega_2, \mu) \\ &\quad + m_{\Lambda_b} f_{\Lambda_b}^{(2)}(\mu) C_{T(\tilde{T})}^B(n \cdot p', \mu) \int_0^\infty d\omega_1 \int_0^\infty d\omega_2 \frac{\psi_4(\omega_1, \omega_2, \mu)}{\omega_1 + \omega_2 - \bar{n} \cdot p' - i0}, \end{aligned} \quad (72)$$

$$\begin{aligned} \Pi_{+, T(\tilde{T})} &= m_{\Lambda_b} f_{\Lambda_b}^{(2)}(\mu) C_{T(\tilde{T})}^A(n \cdot p', \mu) \int_0^\infty d\omega_1 \int_0^\infty d\omega_2 \frac{1}{\omega_1 + \omega_2 - \bar{n} \cdot p' - i0} \\ &\quad J \left( \frac{\mu^2}{\bar{n} \cdot p' \omega_i}, \frac{\omega_i}{\bar{n} \cdot p'} \right) \psi_4(\omega_1, \omega_2, \mu). \end{aligned} \quad (73)$$

### 3.2 Factorization-scale independence

We are now in a position to verify the factorization-scale independence of the correlation functions  $\Pi_{\mu, a}(p, q)$  explicitly at one loop. Having the one-loop factorization formulae at hand we can readily write

$$\begin{aligned} \frac{d}{d \ln \mu} \Pi_{\perp, V(A)} &= \frac{d}{d \ln \mu} \Pi_{\bar{n}, V(A)} \\ &= \frac{\alpha_s(\mu)}{4\pi} \frac{4}{3} \int_0^\infty d\omega_1 \int_0^\infty d\omega_2 \frac{1}{\omega_1 + \omega_2 - \bar{n} \cdot p' - i0} \\ &\quad \times \left[ 4 \ln \frac{\mu}{\omega - \bar{n} \cdot p'} - 4 \ln \frac{\omega - \bar{n} \cdot p'}{\omega_2 - \bar{n} \cdot p'} - 6 \right] \left[ f_{\Lambda_b}^{(2)}(\mu) \psi_4(\omega_1, \omega_2, \mu) \right] \end{aligned}$$

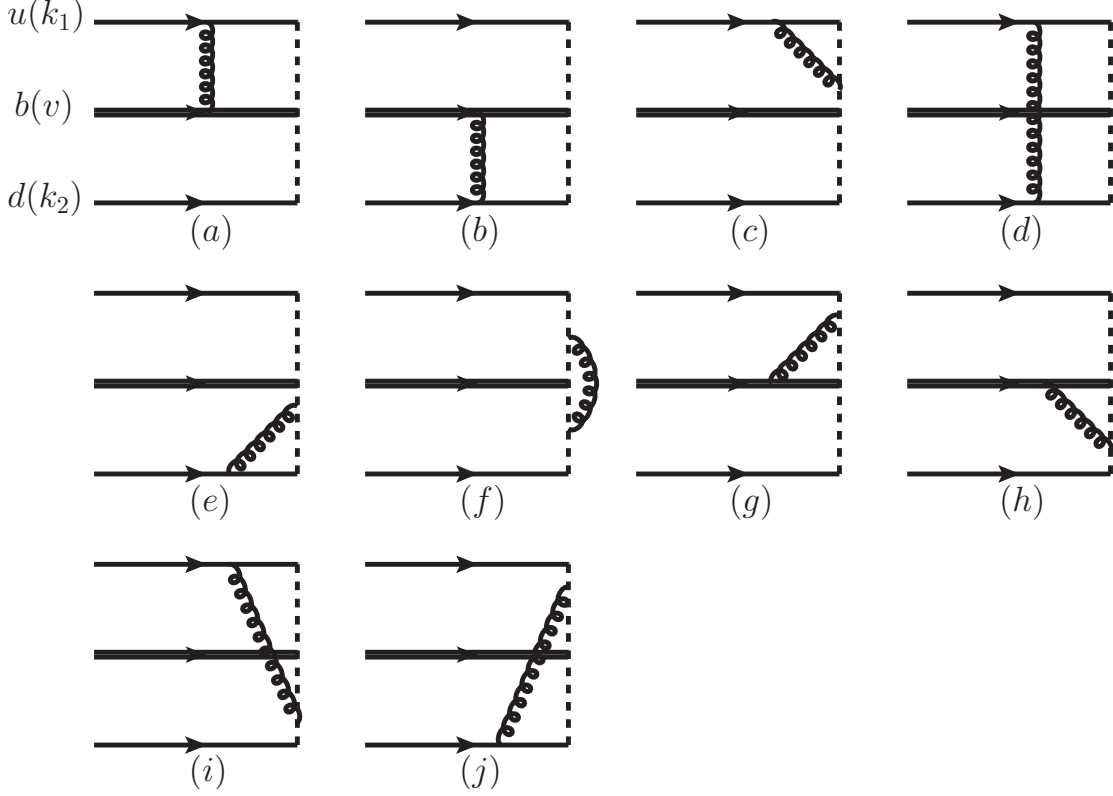


Figure 3: Radiative correction to the  $\Lambda_b$ -baryon DA  $\psi_4(\omega_1, \omega_2, \mu)$  at one loop.

$$+ \int_0^\infty d\omega_1 \int_0^\infty d\omega_2 \frac{1}{\omega_1 + \omega_2 - \bar{n} \cdot p' - i0} \frac{d}{d \ln \mu} \left[ f_{\Lambda_b}^{(2)}(\mu) \psi_4(\omega_1, \omega_2, \mu) \right] + \mathcal{O}(\alpha_s^2), \quad (74)$$

$$\begin{aligned} \frac{d}{d \ln \mu} \Pi_{\perp, T(\tilde{T})} &= \frac{d}{d \ln \mu} \Pi_{+, T(\tilde{T})} \\ &= \frac{d}{d \ln \mu} \Pi_{\perp, V(A)} - \frac{\alpha_s(\mu)}{4\pi} \frac{8}{3} f_{\Lambda_b}^{(2)}(\mu) \int_0^\infty d\omega_1 \int_0^\infty d\omega_2 \frac{\psi_4(\omega_1, \omega_2, \mu)}{\omega_1 + \omega_2 - \bar{n} \cdot p' - i0}, \end{aligned} \quad (75)$$

$$\frac{d}{d \ln \mu} \Pi_{n, V(A)} = \mathcal{O}(\alpha_s^2), \quad (76)$$

where the second term in the evolution equation (75) is due to renormalization of the (pseudo)-tensor currents in QCD, since we do not distinguish the factorization and the renormalization scales in dimensional regularization.

At present the one-loop evolution equation of the  $\Lambda_b$ -baryon DA  $\psi_4(\omega_1, \omega_2, \mu)$  is not explicitly known in the literature, we will compute the factorization-scale dependence of the convolution integral

$$\int_0^\infty d\omega_1 \int_0^\infty d\omega_2 \frac{1}{\omega_1 + \omega_2 - \bar{n} \cdot p' - i0} \frac{d}{d \ln \mu} \left[ f_{\Lambda_b}^{(2)}(\mu) \psi_4(\omega_1, \omega_2, \mu) \right] \quad (77)$$

at one loop in detail. This amounts to extract the UV divergence of the amplitude of the 10 diagrams displayed in Fig. 3.

Applying the Wilson-line Feynman rules we can compute the effective diagram displayed in Fig. 3(a) as

$$\begin{aligned} & \Phi_{bud,a}^{(1)} \otimes T^{(0)} \\ &= -\frac{i}{2} g_s^2 \left(1 + \frac{1}{N_c}\right) \int \frac{d^D l}{(2\pi)^D} \frac{1}{[(k_1 + l)^2 + i0][\bar{n} \cdot (p' - k - l) + i0][-\bar{v} \cdot l + i0][l^2 + i0]} \\ & \quad \epsilon_{ijk} [u_i^T(k_1) C \not{k} (k_1 + l) \gamma_5 \not{l} d_j(k_2)] (1, \gamma_5) \frac{\not{n}}{2} \gamma_\mu (\gamma_{\perp\mu} + \bar{n}_\mu) b_k(v). \end{aligned} \quad (78)$$

Evaluating the loop integral with the standard techniques yields

$$\frac{d}{d \ln \mu} \left[ \Phi_{bud,a}^{(1)} \otimes T^{(0)} \right] = -\frac{\alpha_s(\mu)}{2\pi} \left(1 + \frac{1}{N_c}\right) \frac{\bar{n} \cdot (p' - k)}{\bar{n} \cdot k_1} \ln \frac{\bar{n} \cdot k - \bar{n} \cdot p'}{\bar{n} \cdot k_2 - \bar{n} \cdot p'} \Phi_{bud}^{(0)} \otimes T^{(0)}, \quad (79)$$

which cancels the factorization-scale dependence of the QCD amplitude from the diagram 2(e) in Eq. (57) completely. Based upon the isospin symmetry argument we can readily obtain

$$\frac{d}{d \ln \mu} \left[ \Phi_{bud,b}^{(1)} \otimes T^{(0)} \right] = -\frac{\alpha_s(\mu)}{2\pi} \left(1 + \frac{1}{N_c}\right) \frac{\bar{n} \cdot (p' - k)}{\bar{n} \cdot k_2} \ln \frac{\bar{n} \cdot k - \bar{n} \cdot p'}{\bar{n} \cdot k_1 - \bar{n} \cdot p'} \Phi_{bud}^{(0)} \otimes T^{(0)}. \quad (80)$$

Along the same vein, the light-quark-Wilson-line diagram in Fig. 3(c) can be computed as

$$\begin{aligned} \Phi_{bud,c}^{(1)} \otimes T^{(0)} &= -\frac{i g_s^2 C_F}{\bar{n} \cdot p' - \bar{n} \cdot k + i0} \int \frac{d^D l}{(2\pi)^D} \frac{1}{[(k_1 + l)^2 + i0][\bar{n} \cdot (p' - k - l) + i0][l^2 + i0]} \\ & \quad \epsilon_{ijk} [u_i^T(k_1) C \not{k} (k_1 + l) \gamma_5 \not{l} d_j(k_2)] (1, \gamma_5) \frac{\not{n}}{2} (\gamma_{\perp\mu} + \bar{n}_\mu) b_k(v). \end{aligned} \quad (81)$$

A few comments on evaluating  $\Phi_{bud,c}^{(1)} \otimes T^{(0)}$  are in order.

- The equation of motion for a soft  $u$ -quark field  $u^T(k_1) C \not{k}_1 = 0$  is needed to reduce the Dirac structure of the light-quark sector

$$\begin{aligned} [u_i^T(k_1) C \not{k} (k_1 + l) \gamma_5 \not{l} d_j(k_2)] &= [u_i^T(k_1) C \not{k}_{1\perp} (k_{1\perp} + l_\perp) \gamma_5 \not{l} d_j(k_2)] \\ &\quad \propto 2 \bar{n} \cdot k_1 [u_i^T(k_1) C \gamma_5 \not{l} d_j(k_2)], \end{aligned}$$

where the second step should be understood after performing the integral over the loop momentum  $l$ .

- Since the involved loop integral develops both UV and IR singularities, a fictitious gluon mass  $m_g$  will be introduced to regularize the soft divergence for the sake of separating IR and UV divergences.

- Employing the Georgi parametrization trick leads to

$$\frac{d}{d \ln \mu} \left[ \Phi_{bud,c}^{(1)} \otimes T^{(0)} \right] = \frac{\alpha_s(\mu) C_F}{\pi} \left[ \frac{\bar{n} \cdot (k_2 - p')}{\bar{n} \cdot k_1} \ln \frac{\bar{n} \cdot k_2 - \bar{n} \cdot p'}{\bar{n} \cdot k - \bar{n} \cdot p'} + 1 \right] \Phi_{bud}^{(0)} \otimes T^{(0)}, \quad (82)$$

which further implies that under the isospin symmetry

$$\frac{d}{d \ln \mu} \left[ \Phi_{bud,e}^{(1)} \otimes T^{(0)} \right] = \frac{\alpha_s(\mu) C_F}{\pi} \left[ \frac{\bar{n} \cdot (k_1 - p')}{\bar{n} \cdot k_2} \ln \frac{\bar{n} \cdot k_1 - \bar{n} \cdot p'}{\bar{n} \cdot k - \bar{n} \cdot p'} + 1 \right] \Phi_{bud}^{(0)} \otimes T^{(0)}. \quad (83)$$

- Inspecting the amplitudes of the effective diagrams in Fig. 3(i) and 3(j) yields

$$\Phi_{bud,i}^{(1)} \otimes T^{(0)} = -\frac{1}{2 C_F} \left( 1 + \frac{1}{N_c} \right) \Phi_{bud,c}^{(1)} \otimes T^{(0)}, \quad (84)$$

$$\Phi_{bud,j}^{(1)} \otimes T^{(0)} = -\frac{1}{2 C_F} \left( 1 + \frac{1}{N_c} \right) \Phi_{bud,e}^{(1)} \otimes T^{(0)}. \quad (85)$$

We then conclude that the single logarithmic terms in the evolution equations of

$$\frac{d}{d \ln \mu} \left[ \left( \Phi_{bud,c}^{(1)} + \Phi_{bud,i}^{(1)} \right) \otimes T^{(0)} \right], \quad \frac{d}{d \ln \mu} \left[ \left( \Phi_{bud,e}^{(1)} + \Phi_{bud,j}^{(1)} \right) \otimes T^{(0)} \right] \quad (86)$$

cancel against the ones in the QCD amplitudes for the diagrams 2(b) and 2(c) as presented in (48) and (45), respectively.

We proceed to evaluate the contribution from the effective diagram displayed in Fig. 3(d)

$$\begin{aligned} & \Phi_{bud,d}^{(1)} \otimes T^{(0)} \\ &= -\frac{i}{2} \frac{g_s^2}{\bar{n} \cdot p' - \bar{n} \cdot k + i0} \left( 1 + \frac{1}{N_c} \right) \int \frac{d^D l}{(2\pi)^D} \frac{1}{[(k_1 + l)^2 + i0][(k_2 - l)^2 + i0][l^2 + i0]} \\ & \quad \epsilon_{ijk} \left[ u_i^\Gamma(k_1) C \gamma_\alpha (k_1 + l) \gamma_5 \not{n} (k_2 - l) \gamma^\alpha d_j(k_2) \right] (1, \gamma_5) \frac{\not{\bar{n}}}{2} (\gamma_{\perp\mu} + \bar{n}_\mu) b_k(v). \end{aligned} \quad (87)$$

The factorization-scale dependence of  $\Phi_{bud,d}^{(1)} \otimes T^{(0)}$  can be readily determined as

$$\frac{d}{d \ln \mu} \left[ \Phi_{bud,d}^{(1)} \otimes T^{(0)} \right] = \frac{\alpha_s(\mu)}{4\pi} \left( 1 + \frac{1}{N_c} \right) \Phi_{bud}^{(0)} \otimes T^{(0)}. \quad (88)$$

The self-energy correction to the light-cone Wilson lines shown in Fig. 3(f) vanishes in Feynman gauge due to  $\bar{n}^2 = 0$ .

We further turn to compute the contributions from the heavy-quark-Wilson-line diagrams shown in Fig. 3(g) and (h)

$$\Phi_{bud,g}^{(1)} \otimes T^{(0)} = \Phi_{bud,h}^{(1)} \otimes T^{(0)}$$

$$\begin{aligned}
&= \frac{i}{2} \frac{g_s^2}{\bar{n} \cdot p' - \bar{n} \cdot k + i0} \left(1 + \frac{1}{N_c}\right) \int \frac{d^D l}{(2\pi)^D} \frac{1}{[v \cdot l + i0][\bar{n} \cdot (p' - k + l) + i0][l^2 + i0]} \\
&\quad \epsilon_{ijk} [u_i^T(k_1) C \gamma_5 \not{p} d_j(k_2)] (1, \gamma_5) \frac{\not{p}}{2} \gamma_\mu (\gamma_{\perp\mu} + \bar{n}_\mu) b_k(v).
\end{aligned} \tag{89}$$

Evaluating the UV divergent terms of  $\Phi_{bud,g(h)}^{(1)} \otimes T^{(0)}$  explicitly leads to

$$\begin{aligned}
\frac{d}{d \ln \mu} [\Phi_{bud,g}^{(1)} \otimes T^{(0)}] &= \frac{d}{d \ln \mu} [\Phi_{bud,h}^{(1)} \otimes T^{(0)}] \\
&= -\frac{\alpha_s(\mu)}{2\pi} \left(1 + \frac{1}{N_c}\right) \ln \frac{\mu}{\bar{n} \cdot k - \bar{n} \cdot p'} \Phi_{bud}^{(0)} \otimes T^{(0)},
\end{aligned} \tag{90}$$

which gives the desired cusp anomalous dimension to compensate the corresponding terms in the QCD amplitude of the diagram in Fig. 2(a) as presented in Eqs. (37) and (42).

Finally, we need to consider the LSZ term due to renormalization of the external light quark fields in QCD and of the heavy quark in HQET

$$Z_q = 1 - \frac{\alpha_s(\mu) C_F}{4\pi} \frac{1}{\epsilon}, \quad Z_Q = 1 + \frac{\alpha_s(\mu) C_F}{2\pi} \frac{1}{\epsilon}, \tag{91}$$

which gives rise to

$$\frac{d}{d \ln \mu} [Z_q Z_Q^{1/2} \Phi_{bud}^{(0)} \otimes T^{(0)}] = \mathcal{O}(\alpha_s^2). \tag{92}$$

Putting all the pieces together we obtain

$$\begin{aligned}
&\int_0^\infty d\omega_1 \int_0^\infty d\omega_2 \frac{1}{\omega_1 + \omega_2 - \bar{n} \cdot p' - i0} \frac{d}{d \ln \mu} [f_{\Lambda_b}^{(2)}(\mu) \psi_4(\omega_1, \omega_2, \mu)] \\
&= -\frac{\alpha_s(\mu)}{4\pi} \frac{4}{3} \int_0^\infty d\omega_1 \int_0^\infty d\omega_2 \frac{1}{\omega_1 + \omega_2 - \bar{n} \cdot p' - i0} \\
&\quad \times \left[ 4 \ln \frac{\mu}{\omega - \bar{n} \cdot p'} - 4 \ln \frac{\omega - \bar{n} \cdot p'}{\omega_2 - \bar{n} \cdot p'} - 5 \right] [f_{\Lambda_b}^{(2)}(\mu) \psi_4(\omega_1, \omega_2, \mu)],
\end{aligned} \tag{93}$$

from which we can readily deduce

$$\begin{aligned}
\frac{d}{d \ln \mu} \Pi_{\perp, V(A)} &= \frac{d}{d \ln \mu} \Pi_{\bar{n}, V(A)} \\
&= -\frac{\alpha_s(\mu)}{4\pi} \frac{4}{3} f_{\Lambda_b}^{(2)}(\mu) \int_0^\infty d\omega_1 \int_0^\infty d\omega_2 \frac{\psi_4(\omega_1, \omega_2, \mu)}{\omega_1 + \omega_2 - \bar{n} \cdot p' - i0}.
\end{aligned} \tag{94}$$

The residual  $\mu$ -dependence of  $\Pi_{\perp, V(A)}$  in Eq. (94) stems from the UV renormalization of the baryonic current as displayed in (13). Differentiating the renormalization scales for the interpolating current of the  $\Lambda$ -baryon and for the weak transition current in QCD from the factorization scale (see the next section for details), we reach the desired conclusion that the factorization-scale dependence cancels out completely in the factorized expressions of the correlation functions  $\Pi_{\mu,a}(p, q)$  at one loop.

### 3.3 Resummation of large logarithms

The objective of this section is to sum the parametrically large logarithms to all orders at NLL in perturbative matching coefficients by solving RG evolution equations in momentum space. Following the argument of [12] the characterized scale of the jet function  $\mu_{hc}$  is comparable to the hadronic scale  $\mu_0$  entering the initial condition of the  $\Lambda_b$ -baryon DA in practice, we will not resum logarithms of  $\mu_{hc}/\mu_0$  from the RG running of the hadronic wave function when the factorization scale is chosen as a hard-collinear scale of order  $\sqrt{n \cdot p'} \Lambda$ . Also, the normalization parameter  $f_{\Lambda_b}^{(2)}(\mu)$  will be taken from the HQET sum rule calculation directly instead of converting it to the corresponding QCD coupling, thus in contrast to [12] no RG evolution of  $f_{\Lambda_b}^{(2)}(\mu)$  at the two-loop order is in demand.

Prior to presenting the RG evolution equations of the hard functions we need to distinguish the renormalization and the factorization scales which are set to be equal in dimensional regularization. In doing so we introduce  $\nu$  and  $\nu'$  to denote the renormalization scales for the baryonic current and the weak current in QCD, respectively. It is evident that the dependence of  $\ln \nu$  needs to be separated from the jet function, while the  $\ln \nu'$  dependence requires to be factorized from the hard functions  $C_{T(\bar{T})}^A$ . Following [37] the distinction between the renormalization and the factorization scales can be accounted by writing

$$J\left(\frac{\mu^2}{\bar{n} \cdot p' \omega_i}, \frac{\omega_i}{\bar{n} \cdot p'}, \nu\right) = J\left(\frac{\mu^2}{\bar{n} \cdot p' \omega_i}, \frac{\omega_i}{\bar{n} \cdot p'}\right) + \delta J\left(\frac{\mu^2}{\bar{n} \cdot p' \omega_i}, \frac{\omega_i}{\bar{n} \cdot p'}, \nu\right), \quad (95)$$

$$C_{T(\bar{T})}^A(n \cdot p', \mu, \nu') = C_{T(\bar{T})}^A(n \cdot p', \mu) + \delta C_{T(\bar{T})}^A(n \cdot p', \mu, \nu'), \quad (96)$$

where  $J\left(\frac{\mu^2}{\bar{n} \cdot p' \omega_i}, \frac{\omega_i}{\bar{n} \cdot p'}\right)$  and  $C_{T(\bar{T})}^A(n \cdot p', \mu)$  on the right-hand sides refer to the matching coefficients given by Eqs. (66) and (69). Exploiting the RG evolution equations

$$\frac{d}{d \ln \nu} \ln \delta J\left(\frac{\mu^2}{\bar{n} \cdot p' \omega_i}, \frac{\omega_i}{\bar{n} \cdot p'}, \nu\right) = - \sum_k \left(\frac{\alpha_s(\mu)}{4\pi}\right)^k \gamma_{\Lambda}^{(k)}, \quad (97)$$

$$\frac{d}{d \ln \nu'} \ln \delta C_{T(\bar{T})}^A(n \cdot p', \mu, \nu') = - \sum_k \left(\frac{\alpha_s(\mu)}{4\pi}\right)^k \gamma_{T(\bar{T})}^{(k)}, \quad (98)$$

and implementing the renormalization conditions

$$\delta J\left(\frac{\mu^2}{\bar{n} \cdot p' \omega_i}, \frac{\omega_i}{\bar{n} \cdot p'}, \mu\right) = 0, \quad \delta C_{T(\bar{T})}^A(n \cdot p', \mu, \mu) = 0, \quad (99)$$

we find

$$\delta J\left(\frac{\mu^2}{\bar{n} \cdot p' \omega_i}, \frac{\omega_i}{\bar{n} \cdot p'}, \nu\right) = - \left(\frac{\alpha_s(\mu)}{4\pi}\right) \gamma_{\Lambda}^{(1)} \ln \frac{\nu}{\mu} + \mathcal{O}(\alpha_s^2), \quad (100)$$

$$\delta C_{T(\bar{T})}^A(n \cdot p', \mu, \nu') = - \left(\frac{\alpha_s(\mu)}{4\pi}\right) \gamma_{T(\bar{T})}^{(1)} \ln \frac{\nu'}{\mu} + \mathcal{O}(\alpha_s^2), \quad (101)$$

The anomalous dimensions  $\gamma_\Lambda^{(k)}$  are already defined in Eq. (13), and the renormalization constants  $\gamma_{T(\tilde{T})}^{(k)}$  at two loops are given by [37]

$$\gamma_{T(\tilde{T})}^{(1)} = 2 C_F, \quad \gamma_{T(\tilde{T})}^{(2)} = -C_F \left[ 19 C_F - \frac{257}{9} C_A + \frac{52}{9} n_f T_F \right], \quad (102)$$

where  $n_f = 5$  denotes the number of active quark flavours.

Now we are ready to present the jet function and the hard function for the weak tensor current with the renormalization scales distinct from the factorization scale

$$\begin{aligned} & J \left( \frac{\mu^2}{\bar{n} \cdot p' \omega_i}, \frac{\omega_i}{\bar{n} \cdot p'}, \nu \right) \\ &= 1 + \frac{\alpha_s(\mu)}{4\pi} \frac{4}{3} \left\{ \ln^2 \frac{\mu^2}{n \cdot p' (\omega - \bar{n} \cdot p')} - 2 \ln \frac{\omega - \bar{n} \cdot p'}{\omega_2 - \bar{n} \cdot p'} \ln \frac{\mu^2}{n \cdot p' (\omega - \bar{n} \cdot p')} \right. \\ &\quad - \frac{1}{2} \ln \frac{\nu^2}{n \cdot p' (\omega - \bar{n} \cdot p')} - \ln^2 \frac{\omega - \bar{n} \cdot p'}{\omega_2 - \bar{n} \cdot p'} + 2 \ln \frac{\omega - \bar{n} \cdot p'}{\omega_2 - \bar{n} \cdot p'} \left[ \frac{\omega_2 - \bar{n} \cdot p'}{\omega_1} - \frac{3}{4} \right] \\ &\quad \left. - \frac{\pi^2}{6} - \frac{1}{2} \right\}, \end{aligned} \quad (103)$$

$$\begin{aligned} & C_{T(\tilde{T})}^A(n \cdot p', \mu, \nu') \\ &= 1 - \frac{\alpha_s(\mu) C_F}{4\pi} \left[ 2 \ln^2 \frac{\mu}{n \cdot p'} + 5 \ln \frac{\mu}{m_b} + 2 \ln \frac{\nu'}{m_b} - 2 \text{Li}_2 \left( 1 - \frac{1}{r} \right) - \ln^2 r \right. \\ &\quad \left. + \frac{4r-2}{1-r} \ln r + \frac{\pi^2}{12} + 6 \right]. \end{aligned} \quad (104)$$

Resummation of large logarithms in the hard functions at NLL can be achieved by solving the RG equations

$$\frac{d}{d \ln \mu} C_i(n \cdot p', \mu, \nu') = \left[ -\Gamma_{\text{cusp}}(\alpha_s) \ln \frac{\mu}{n \cdot p'} + \gamma(\alpha_s) \right] C_i(n \cdot p', \mu, \nu'), \quad (105)$$

$$\frac{d}{d \ln \nu'} C_{T(\tilde{T})}^A(n \cdot p', \mu, \nu') = \left[ -\sum_k \left( \frac{\alpha_s(\mu)}{4\pi} \right)^k \gamma_{T(\tilde{T})}^{(k)} \right] C_{T(\tilde{T})}^A(n \cdot p', \mu, \nu'), \quad (106)$$

where  $C_i$  stands for  $C_{\perp, V(A)}$ ,  $C_{\bar{n}, V(A)}$  and  $C_{T(\tilde{T})}^A$ , the cusp anomalous dimension  $\Gamma_{\text{cusp}}(\alpha_s)$  at the three-loop order and the remaining anomalous dimensions  $\gamma(\alpha_s)$  and  $\gamma_{T(\tilde{T})}^{(k)}$  at two loops are needed (see [38] for the detailed expressions). Solving Eqs. (105) and (106) yields

$$C_{\perp(\bar{n}), V(A)}(n \cdot p', \mu) = U_1(\bar{n} \cdot p'/2, \mu_h, \mu) C_{\perp(\bar{n}), V(A)}(n \cdot p', \mu_h), \quad (107)$$

$$C_{T(\tilde{T})}^A(n \cdot p', \mu, \nu') = U_1(\bar{n} \cdot p'/2, \mu_h, \mu) U_2(\nu'_h, \nu') C_{T(\tilde{T})}^A(n \cdot p', \mu_h, \nu'_h), \quad (108)$$



where  $U_1(\bar{n} \cdot p'/2, \mu_h, \mu)$  can be deduced from  $U_1(E_\gamma, \mu_h, \mu)$  in [38] with  $E_\gamma \rightarrow \bar{n} \cdot p'/2$ , and  $U_2(\nu'_h, \nu')$  can be read from  $U_2(\mu_{h2}, \mu)$  in [12] with the following substituent rules

$$\mu_{h2} \rightarrow \nu'_h, \quad \mu \rightarrow \nu', \quad \tilde{\gamma}^{(k)} \rightarrow -\gamma_{T(\bar{T})}^{(k-1)}. \quad (109)$$

Finally we present NLL resummation improved factorized formulae for the invariant amplitudes entering the Lorenz decomposition of the correlation functions  $\Pi_{\mu,a}(p, q)$

$$\begin{aligned} \Pi_{\perp, V(A)} &= f_{\Lambda_b}^{(2)}(\mu) [U_1(\bar{n} \cdot p'/2, \mu_h, \mu) C_{\perp, V(A)}(n \cdot p', \mu_h)] \\ &\int_0^\infty d\omega_1 \int_0^\infty d\omega_2 \frac{1}{\omega_1 + \omega_2 - \bar{n} \cdot p' - i0} J\left(\frac{\mu^2}{\bar{n} \cdot p' \omega_i}, \frac{\omega_i}{\bar{n} \cdot p'}, \nu\right) \psi_4(\omega_1, \omega_2, \mu), \end{aligned} \quad (110)$$

$$\begin{aligned} \Pi_{\bar{n}, V(A)} &= f_{\Lambda_b}^{(2)}(\mu) [U_1(\bar{n} \cdot p'/2, \mu_h, \mu) C_{\bar{n}, V(A)}(n \cdot p', \mu_h)] \\ &\int_0^\infty d\omega_1 \int_0^\infty d\omega_2 \frac{1}{\omega_1 + \omega_2 - \bar{n} \cdot p' - i0} J\left(\frac{\mu^2}{\bar{n} \cdot p' \omega_i}, \frac{\omega_i}{\bar{n} \cdot p'}, \nu\right) \psi_4(\omega_1, \omega_2, \mu), \end{aligned} \quad (111)$$

$$\begin{aligned} \Pi_{\perp, T(\bar{T})} &= m_{\Lambda_b} f_{\Lambda_b}^{(2)}(\mu) [U_1(\bar{n} \cdot p'/2, \mu_h, \mu) U_2(\nu'_h, \nu') C_{T(\bar{T})}^A(n \cdot p', \mu_h, \nu'_h)] \\ &\int_0^\infty d\omega_1 \int_0^\infty d\omega_2 \frac{1}{\omega_1 + \omega_2 - \bar{n} \cdot p' - i0} J\left(\frac{\mu^2}{\bar{n} \cdot p' \omega_i}, \frac{\omega_i}{\bar{n} \cdot p'}, \nu\right) \psi_4(\omega_1, \omega_2, \mu) \\ &+ m_{\Lambda_b} f_{\Lambda_b}^{(2)}(\mu) C_{T(\bar{T})}^B(n \cdot p', \mu) \int_0^\infty d\omega_1 \int_0^\infty d\omega_2 \frac{\psi_4(\omega_1, \omega_2, \mu)}{\omega_1 + \omega_2 - \bar{n} \cdot p' - i0}. \end{aligned} \quad (112)$$

where  $\mu$  needs to be taken as a hard-collinear scale of order  $\sqrt{n \cdot p'} \Lambda$  and  $\mu_h$  should be set to a hard scale of order  $n \cdot p' \sim m_b$ . Choosing  $\nu'_h = m_b$  to eliminate the single logarithmic term  $\ln(\nu'_h/m_b)$  in  $C_{T(\bar{T})}^A(n \cdot p', \mu_h, \nu'_h)$ , the evolution function  $U_2(\nu'_h, \nu')$  can be further reduced to one provided that  $\nu' = m_b$ .

## 4 The LCSR of $\Lambda_b \rightarrow \Lambda$ form factors at $\mathcal{O}(\alpha_s)$

It is now a straightforward task to derive the NLL resummation improved sum rules for the  $\Lambda_b \rightarrow \Lambda$  form factors. Working out dispersion forms of the factorized correlation functions with the aid of the relations in Appendix A and applying the standard strategies to construct QCD sum rules, we find

$$\begin{aligned} &f_\Lambda(\nu) (n \cdot p') e^{-m_\Lambda^2/(n \cdot p' \omega_M)} \{f_{\Lambda_b \rightarrow \Lambda}^T(q^2), g_{\Lambda_b \rightarrow \Lambda}^T(q^2)\} \\ &= f_{\Lambda_b}^{(2)}(\mu) [U_1(\bar{n} \cdot p'/2, \mu_h, \mu) C_{\perp, V(A)}(n \cdot p', \mu_h)] \int_0^{\omega_s} d\omega' e^{-\omega'/\omega_M} \psi_{4,\text{eff}}(\omega', \mu, \nu), \quad (113) \\ &f_\Lambda(\nu) (n \cdot p') e^{-m_\Lambda^2/(n \cdot p' \omega_M)} \{f_{\Lambda_b \rightarrow \Lambda}^0(q^2), g_{\Lambda_b \rightarrow \Lambda}^0(q^2)\} \\ &= f_{\Lambda_b}^{(2)}(\mu) [U_1(\bar{n} \cdot p'/2, \mu_h, \mu) C_{\bar{n}, V(A)}(n \cdot p', \mu_h)] \int_0^{\omega_s} d\omega' e^{-\omega'/\omega_M} \psi_{4,\text{eff}}(\omega', \mu, \nu) \end{aligned}$$

$$+ f_{\Lambda_b}^{(2)}(\mu) \left(1 - \frac{n \cdot p'}{m_{\Lambda_b}}\right) C_{n,V(A)}(n \cdot p', \mu_h) \int_0^{\omega_s} d\omega' e^{-\omega'/\omega_M} \tilde{\psi}_4(\omega', \mu), \quad (114)$$

$$\begin{aligned} & f_\Lambda(\nu) (n \cdot p') e^{-m_\Lambda^2/(n \cdot p' \omega_M)} \{f_{\Lambda_b \rightarrow \Lambda}^+(q^2), g_{\Lambda_b \rightarrow \Lambda}^+(q^2)\} \\ &= f_{\Lambda_b}^{(2)}(\mu) [U_1(\bar{n} \cdot p'/2, \mu_h, \mu) C_{\bar{n},V(A)}(n \cdot p', \mu_h)] \int_0^{\omega_s} d\omega' e^{-\omega'/\omega_M} \psi_{4,\text{eff}}(\omega', \mu, \nu) \\ &\quad - f_{\Lambda_b}^{(2)}(\mu) \left(1 - \frac{n \cdot p'}{m_{\Lambda_b}}\right) C_{n,V(A)}(n \cdot p', \mu_h) \int_0^{\omega_s} d\omega' e^{-\omega'/\omega_M} \tilde{\psi}_4(\omega', \mu), \end{aligned} \quad (115)$$

$$\begin{aligned} & f_\Lambda(\nu) (n \cdot p') e^{-m_\Lambda^2/(n \cdot p' \omega_M)} \{h_{\Lambda_b \rightarrow \Lambda}^T(q^2), \tilde{h}_{\Lambda_b \rightarrow \Lambda}^T(q^2)\} \\ &= f_{\Lambda_b}^{(2)}(\mu) \left\{ \left[ U_1(\bar{n} \cdot p'/2, \mu_h, \mu) U_2(\nu'_h, \nu') C_{T(\bar{T})}^A(n \cdot p', \mu_h, \nu'_h) \right] + C_{T(\bar{T})}^B(n \cdot p', \mu) \right\} \\ &\quad \times \int_0^{\omega_s} d\omega' e^{-\omega'/\omega_M} \psi_{4,\text{eff}}(\omega', \mu, \nu), \end{aligned} \quad (116)$$

$$\begin{aligned} & f_\Lambda(\nu) (n \cdot p') e^{-m_\Lambda^2/(n \cdot p' \omega_M)} \{h_{\Lambda_b \rightarrow \Lambda}^+(q^2), \tilde{h}_{\Lambda_b \rightarrow \Lambda}^+(q^2)\} \\ &= f_{\Lambda_b}^{(2)}(\mu) \left[ U_1(\bar{n} \cdot p'/2, \mu_h, \mu) U_2(\nu'_h, \nu') C_{T(\bar{T})}^A(n \cdot p', \mu_h, \nu'_h) \right] \\ &\quad \times \int_0^{\omega_s} d\omega' e^{-\omega'/\omega_M} \psi_{4,\text{eff}}(\omega', \mu, \nu), \end{aligned} \quad (117)$$

where we need to multiply out all  $[1 + \mathcal{O}(\alpha_s)]$  factors involved in the NLO perturbative matching coefficients and the RG evolution functions, and drop out  $\mathcal{O}(\alpha_s^2)$  terms beyond the NLL approximation [38]. The effective ‘‘distribution amplitude’’  $\psi_{4,\text{eff}}(\omega', \mu, \nu)$  is given by

$$\begin{aligned} \psi_{4,\text{eff}}(\omega', \mu, \nu) &= \tilde{\psi}_4(\omega', \mu) + \frac{\alpha_s(\mu)}{4\pi} \frac{4}{3} \left\{ \int_0^{\omega'} d\omega \left[ \frac{2}{\omega' - \omega} \ln \frac{\mu^2}{n \cdot p' (\omega' - \omega)} \right]_{\oplus} \tilde{\psi}_4(\omega, \mu) \right. \\ &\quad - 2\omega' \int_0^{\omega'} d\omega \left[ \frac{1}{\omega' - \omega} \ln \frac{\omega' - \omega}{\omega'} \right]_{\oplus} \phi_4(\omega, \mu) \\ &\quad - \omega' \int_{\omega'}^{\infty} d\omega \left[ \frac{\omega}{\omega'} \ln^2 \frac{\mu^2}{n \cdot p' \omega'} - 2 \ln \frac{\mu^2}{n \cdot p' \omega'} \ln \frac{\omega - \omega'}{\omega'} - \frac{11}{2} \ln \frac{\omega - \omega'}{\omega'} \right. \\ &\quad \quad \left. - \frac{\pi^2 + 1}{2} \frac{\omega}{\omega'} + \left( \frac{2\pi^2}{3} - \frac{11}{2} \right) \right] \frac{d\phi_4(\omega, \mu)}{d\omega} \\ &\quad - \int_{\omega'}^{\infty} \left[ \ln^2 \frac{\mu^2}{n \cdot p' \omega'} + 2 \ln \frac{\omega - \omega'}{\omega} - \frac{\pi^2 + 1}{2} \right] \phi_4(\omega, \mu) \\ &\quad \left. - \int_0^{\omega'} d\omega \left[ 2 \ln^2 \frac{\mu^2}{n \cdot p' (\omega' - \omega)} + \frac{1}{2} \ln^2 \frac{\nu^2}{n \cdot p' (\omega' - \omega)} \right] \frac{d\tilde{\psi}_4(\omega, \mu)}{d\omega} \right\}, \end{aligned} \quad (118)$$

where  $\psi_4(\omega_1, \omega_2, \mu) = \psi_4(u\omega, (1-u)\omega, \mu)$  is supposed to be independent of the momentum fraction  $u$  as motivated by [2, 14, 18] and will be set to  $\phi_4(\omega, \mu)$  for brevity, and  $\tilde{\psi}_4(\omega, \mu)$

defined in Eq. (30) can be identified as  $\tilde{\psi}_4(\omega, \mu) = \omega \phi_4(\omega, \mu)$  within this approximation. The  $\oplus$  function is defined as

$$\int_0^\infty d\omega [f(\omega, \omega')]_{\oplus} g(\omega) = \int_0^\infty d\omega f(\omega, \omega') [g(\omega) - g(\omega')]. \quad (119)$$

The following observations on the structures of the NLL sum rules can be made.

- Due to the integration bounds of  $\omega'$  after the continuum subtraction, the scaling behaviour  $\omega' \sim \omega_s \sim \Lambda^2/(n \cdot p')$  implies that the natural choice for the factorization scale  $\mu$  of  $\ln^k [\mu^2/(n \cdot p' \omega')]$  ( $k = 1, 2$ ) in  $\psi_{4,\text{eff}}(\omega', \mu, \nu)$  should be  $\mu_s \sim s_0 = n \cdot p' \omega' \sim \Lambda^2$  in contrast to the favored choice  $\mu_{hc} \sim n \cdot p' \Lambda$  in the factorization formulae of the correlation functions presented in Eqs. (110), (111) and (112).
- Due to the power counting  $\omega \sim \Lambda$  determined by the canonical behaviour of the  $\Lambda_b$ -baryon DA  $\phi_4(\omega, \mu)$ , the logarithmic term  $\ln[(\omega - \omega')/\omega']$  appeared in  $\psi_{4,\text{eff}}(\omega', \mu, \nu)$  is counted as  $\ln(n \cdot p'/\Lambda)$  in the heavy-quark limit. Such enhanced logarithm arises from the contributions of the  $\Lambda$ -baryon vertex diagrams and the two box diagrams displayed in Fig. 2 and it shares the same origin as the rapidity singularities preventing a complete factorization of heavy-to-light form factors in SCET<sub>II</sub> (see also [10]). It is evident that the standard momentum-space resummation technique cannot be applied to cope with this term which is independent of the factorization scale. Investigating resummation of such logarithm with the rapidity RG evolution equations [39–42] is apparently of conceptual interest and we will pursue this endeavour in a future work.

## 5 Numerical results

Having at hand the NLL resummation improved sum rules for the  $\Lambda_b \rightarrow \Lambda$  form factors we are ready to explore their phenomenological implications. We will begin the numerical analysis with specifying the non-perturbative models for the  $\Lambda_b$ -baryon DA, determining the “internal” sum rule parameters and evaluating the normalization parameters  $f_\Lambda(\nu)$  and  $f_{\Lambda_b}^{(2)}(\mu)$ . Theory predictions for the  $\Lambda_b \rightarrow \Lambda$  form factors at large hadronic recoil will be further presented and extrapolation of the form factors toward large momentum transfer will be performed by applying the  $z$ -series expansion and matching the calculated form factors from the LCSR approach at low  $q^2$ .

### 5.1 Theory input parameters

Light-cone wave functions of the  $\Lambda_b$ -baryon at small transverse separations have attracted renewed attention [14, 18, 19] due to the available measurements of the baryonic  $\Lambda_b \rightarrow \Lambda \ell^+ \ell^-$  decays at the LHC and the Tevatron [43–45]. Improved models of the twist-2  $\Lambda_b$ -baryon DA in compatible with the RG evolution equation at one loop have been discussed in [18, 19], however, no dedicated study of the twist-4 DA  $\psi_4(\omega_1, \omega_2, \mu)$  (or  $\phi_4(\omega, \mu)$ ), taking into account the QCD constraints, exists in the literature to the best of our knowledge. Motivated by the

“on-shell-wave-function” analysis of [18] we consider three different parameterizations of the  $\Lambda_b$ -baryon DA  $\phi_4(\omega, \mu_0)$  at a soft scale

$$\begin{aligned}\phi_4^{\text{I}}(\omega, \mu_0) &= \frac{1}{\omega_0^2} e^{-\omega/\omega_0}, \\ \phi_4^{\text{II}}(\omega, \mu_0) &= \frac{1}{\omega_0^2} e^{-(\omega/\omega_1)^2}, \quad \omega_1 = \sqrt{2}\omega_0, \\ \phi_4^{\text{III}}(\omega, \mu_0) &= \frac{1}{\omega_0^2} \left[ 1 - \sqrt{\left(2 - \frac{\omega}{\omega_2}\right) \frac{\omega}{\omega_2}} \right] \theta(\omega_2 - \omega), \quad \omega_2 = \sqrt{\frac{12}{10 - 3\pi}}\omega_0,\end{aligned}\quad (120)$$

where  $\phi_4^{\text{II}}(\omega, \mu_0)$  and  $\phi_4^{\text{III}}(\omega, \mu_0)$  are analogies to the mesonic counterparts proposed in [10] for the sake of maximizing the model dependence of  $\phi_4(\omega, \mu_0)$  and the normalization constants are determined by

$$\int_0^\infty d\omega \omega \phi_4(\omega, \mu) = 1. \quad (121)$$

Applying the equations of motion with the Wandzura-Wilczek approximation yields

$$\psi_2(\omega_1, \omega_2, \mu_0) = \omega_1 \omega_2 \frac{d\psi_4(\omega_1, \omega_2, \mu_0)}{d\omega_1 d\omega_2}, \quad (122)$$

in analogy to the Wandzura-Wilczek relation for the  $B$ -meson DA [46]. We will take  $\phi_4^{\text{I}}(\omega, \mu_0)$  as our default model in computing the  $\Lambda_b \rightarrow \Lambda$  form factors from the LCSR approach and take into account the numerical impact of the alternative parameterizations  $\phi_4^{\text{II,III}}(\omega, \mu_0)$  in the uncertainty analysis. To illustrate the main features of the above-mentioned three models we present the small  $\omega$  behaviors of  $\phi_4(\omega, \mu_0)$  in Fig. 4 with a reference value  $\omega_0 = 280$  MeV. We remark that these models do not develop the radiative tail at large  $\omega$  due to perturbative corrections, and they should be merely treated as an effective description of  $\phi_4(\omega, \mu_0)$  at small  $\omega$  where QCD factorization of the correlation functions is established.

Regarding the determination of the internal sum rule parameters we follow closely the strategies proposed to explore the sum rules for the  $B \rightarrow \pi$  form factors [12].

- To reduce the systematic uncertainty induced by the parton-hadron duality approximation, the continuum contributions to the dispersion forms of the correlation functions, displayed in Eqs. (110), (111), (112), (62) and (73) need to be under reasonable control, i.e., less than 40 %.
- The sum rule predictions should be stable with respect to the variation of the Borel mass parameter  $\omega_M$ . More concretely, we impose the following condition on the logarithmic derivative to a given form factor

$$\frac{\partial \ln F_{\Lambda_b \rightarrow \Lambda}^i}{\partial \ln \omega_M} \leq 40\%, \quad (123)$$

where  $F_{\Lambda_b \rightarrow \Lambda}^i$  stands for a general  $\Lambda_b \rightarrow \Lambda$  form factor.

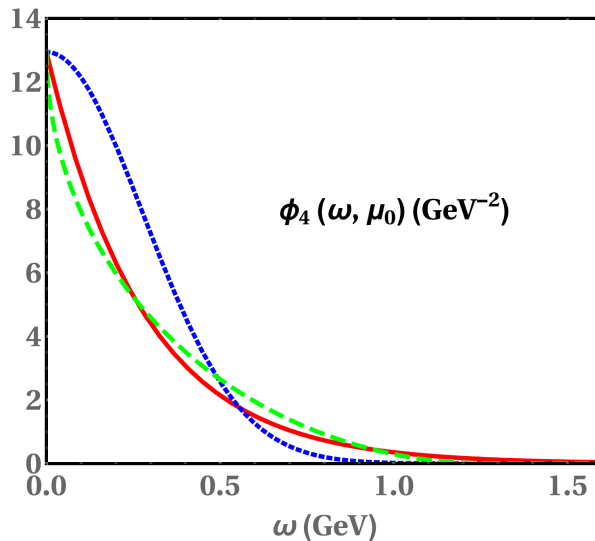


Figure 4: The small  $\omega$  behaviors for three different models of  $\phi_4(\omega, \mu_0)$ . Solid (red), dotted (blue) and dashed (green) curves refer to  $\phi_4^{\text{I}}$ ,  $\phi_4^{\text{II}}$  and  $\phi_4^{\text{III}}$ , respectively.

The allowed regions of the Borel parameter and the effective duality threshold are found to be

$$M^2 \equiv n \cdot p' \omega_M = (2.6 \pm 0.4) \text{ GeV}^2, \quad s_0 \equiv n \cdot p' \omega_s = (2.56 \pm 0.10) \text{ GeV}^2, \quad (124)$$

where the obtained interval of  $s_0$  is in agreement with that adopted in [2, 23].

The coupling  $f_{\Lambda_b}^{(2)}(\mu_0)$  will be taken from the NLO HQET sum rule calculation [47]

$$f_{\Lambda_b}^{(2)}(1 \text{ GeV}) = (3.0 \pm 0.5) \times 10^{-2} \text{ GeV}^3. \quad (125)$$

In order to reduce the theory uncertainty induced by the Borel mass parameter  $\omega_M$  we will employ the two-point QCD sum rules of the normalization parameter  $f_\Lambda(\nu)$  [48]

$$f_\Lambda^2 e^{-m_\Lambda^2/M^2} = \frac{1}{640 \pi^4} \int_{m_s^2}^{s_0} ds e^{-s/M^2} s \left(1 - \frac{m_s^2}{s}\right)^5 - \frac{1}{192 \pi^2} \left\langle \frac{\alpha_s}{\pi} GG \right\rangle \int_{m_s^2}^{s_0} ds e^{-s/M^2} \frac{m_s^2}{s^2} \left(1 - \frac{m_s^2}{s}\right) \left(1 - \frac{2m_s^2}{s}\right) \quad (126)$$

at tree level, where the gluon condensate density  $\langle \alpha_s/\pi GG \rangle = (1.2_{-1.2}^{+0.6}) \times 10^{-2} \text{ GeV}^4$  will be used in the numerical analysis.

We now turn to discuss the choices of the renormalization and the factorization scales entering the NLL sum rules. The renormalization scale  $\nu$  of the baryonic current and the factorization scale  $\mu$  will be varied in the interval  $1 \text{ GeV} \leq \mu, \nu \leq 2 \text{ GeV}$  around the default

value  $\mu = \nu = 1.5 \text{ GeV}$ . The renormalization scale  $\nu'$  of the weak (pseudo)-tensor currents and the hard scale  $\mu_h$  in the hard matching coefficients will be taken as  $\mu_h = \nu' = m_b$  with the variation in the range  $[m_b/2, 2m_b]$ . In addition, we adopt the  $\overline{\text{MS}}$  bottom-quark mass  $\overline{m}_b(\overline{m}_b) = 4.193_{-0.035}^{+0.022} \text{ GeV}$  determined from non-relativistic sum rules for the inclusive  $e^+ e^- \rightarrow b\bar{b}$  production cross section at next-to-next-to-next-to-leading order [49].

## 5.2 Predictions for the $\Lambda_b \rightarrow \Lambda$ form factors

After specifying all the necessary input parameters we will first turn to determine the shape parameter  $\omega_0$  of the  $\Lambda_b$ -baryon DA  $\phi_4(\omega, \mu_0)$ . Given the sizeable uncertainty of  $\omega_0$  estimated from the sum rule analysis in [14], we prefer to, following [12], extract this parameter by matching the LCSR prediction of the form factor  $f_{\Lambda_b \rightarrow \Lambda}^+(q^2)$  at zero momentum transfer to that determined from an alternative method. In doing so, we apply the SU(3) flavour symmetry relation between the  $\Lambda_b \rightarrow \Lambda$  and the  $\Lambda_b \rightarrow p$  form factors

$$\frac{f_{\Lambda_b \rightarrow \Lambda}^+(0)}{f_{\Lambda_b \rightarrow p}^+(0)} \simeq \frac{f_\Lambda}{f_N}, \quad (127)$$

motivated by an analogous relation for the  $B$ -meson decay form factors

$$\frac{f_{B \rightarrow K}^+(0)}{f_{B \rightarrow \pi}^+(0)} \simeq \frac{f_K}{f_\pi}, \quad (128)$$

which turns out to be a rather satisfactory approximation when confronted with the predictions from both the LCSR [50, 51] and the TMD factorization [52, 53] approaches. Employing the prediction of  $f_{\Lambda_b \rightarrow p}^+(0)$  from the LCSR with the nucleon DA [29] and the result of  $f_\Lambda/f_N$  computed from QCD sum rules [30] yields  $f_{\Lambda_b \rightarrow \Lambda}^+(0) = 0.18 \pm 0.04$ . Proceeding with the above-mentioned matching procedure we then find

$$\begin{aligned} \omega_0 &= 280_{-38}^{+47} \text{ MeV}, & (\text{Model I}) \\ \omega_0 &= 386_{-37}^{+45} \text{ MeV}, & (\text{Model II}) \\ \omega_0 &= 273_{-29}^{+38} \text{ MeV}. & (\text{Model III}) \end{aligned} \quad (129)$$

The apparent dependence of the extracted values of  $\omega_0$  on the specific parametrization of  $\phi_4(\omega, \mu_0)$  implies that the  $\Lambda_b \rightarrow \Lambda$  form factors cannot be determined by the shape parameter  $\omega_0$  satisfactorily to a reasonable approximation and the detailed information of the small  $\omega$  behaviours of  $\phi_4(\omega, \mu_0)$  is in demand to have a better control on the form factors from the sum rule analysis. Having this in mind, our main purpose is to predict the momentum-transfer dependence of all the ten  $\Lambda_b \rightarrow \Lambda$  form factors in anticipation of the reduced model dependence of  $\phi_4(\omega, \mu_0)$  in the form factor ratios. Anatomy of the sum rules numerically indeed indicates the expected insensitivity of the form-factor shapes as displayed in Fig. 5.

To demonstrate some important numerical features of the LCSR predictions, we show the dependencies of  $f_{\Lambda_b \rightarrow \Lambda}^T(0)$  on the sum rule parameters  $M^2$  and  $s_0$  and on the factorization scale  $\mu$  in Fig. 6 as an illustrative example and analogous profiles are also observed for the remaining

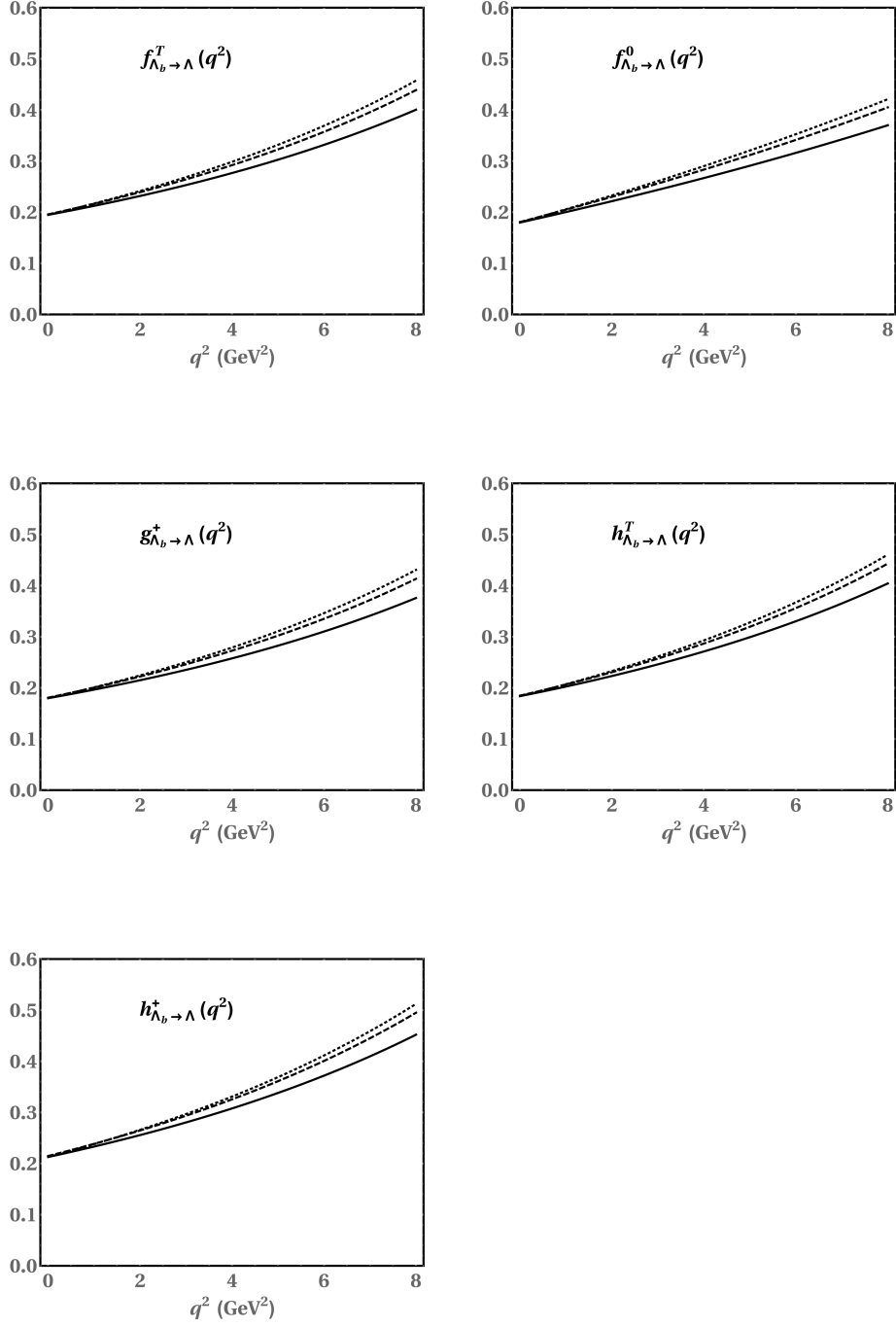


Figure 5: The momentum-transfer dependence of the  $\Lambda_b \rightarrow \Lambda$  form factors computed from LCSR with the fitted values of  $\omega_0$  parameter presented in (129) for three different models of  $\phi_4(\omega, \mu_0)$ . Solid, dotted and dashed curves correspond to the sum rule predictions with the  $\Lambda_b$ -baryon DA  $\phi_4^{\text{I}}(\omega, \mu_0)$ ,  $\phi_4^{\text{II}}(\omega, \mu_0)$  and  $\phi_4^{\text{III}}(\omega, \mu_0)$ , respectively.

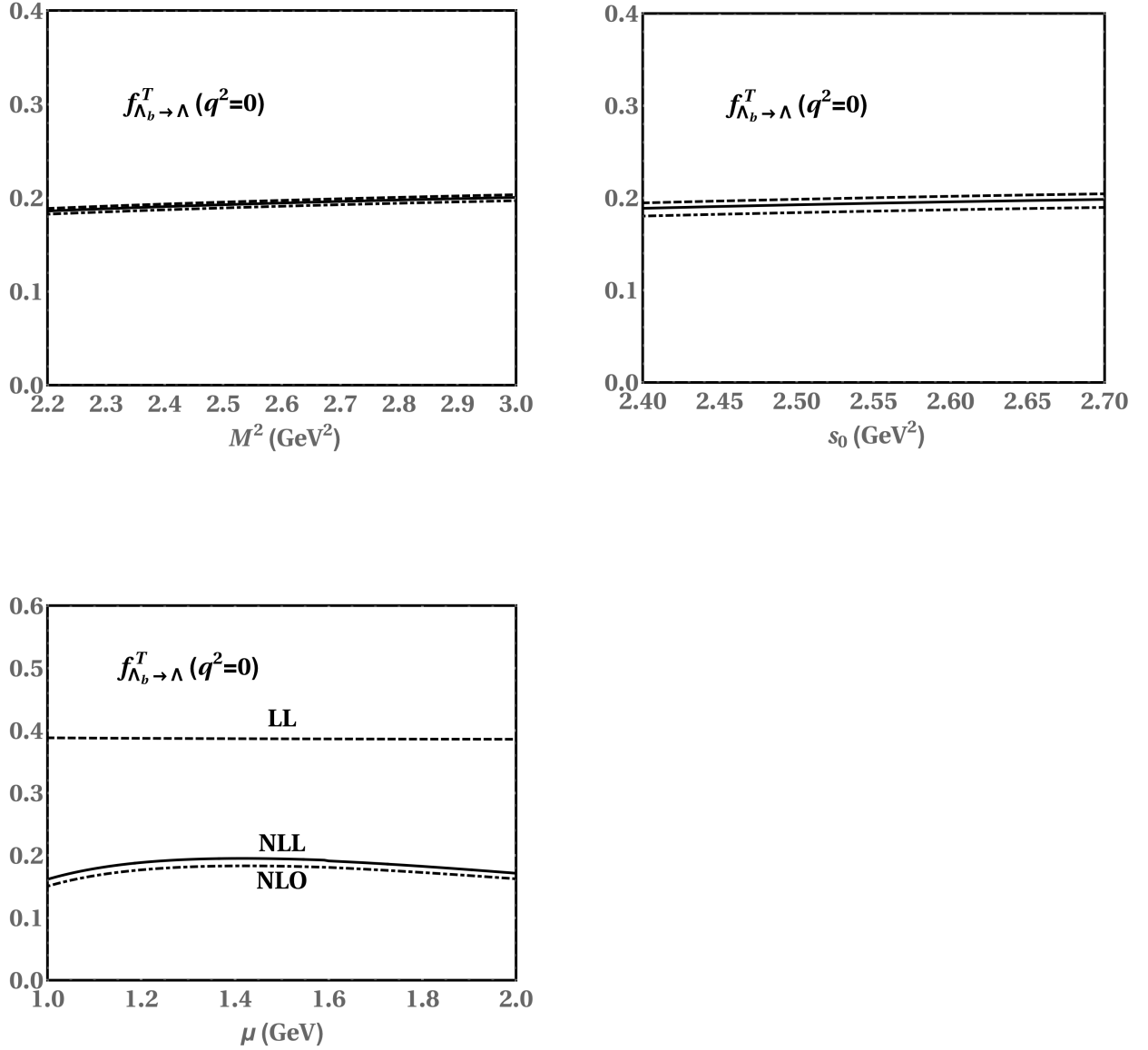


Figure 6: Dependence of  $f_{\Lambda_b \to \Lambda}^T(0)$  on the Borel parameter (top left), on the threshold parameter (top right) and on the factorization scale (bottom left). Solid, dashed and dotted curves are obtained from the NLL sum rules with  $s_0 = 2.56$  GeV<sup>2</sup>,  $2.66$  GeV<sup>2</sup>,  $2.46$  GeV<sup>2</sup> (top left) and  $M^2 = 2.6$  GeV<sup>2</sup>,  $3.0$  GeV<sup>2</sup>,  $2.2$  GeV<sup>2</sup> (top right) while all the other input parameters are fixed at their central values. The curves labelled by “LL”, “NLO” and “NLL” (bottom) correspond to the sum rule predictions at LL, NLO and NLL accuracy.



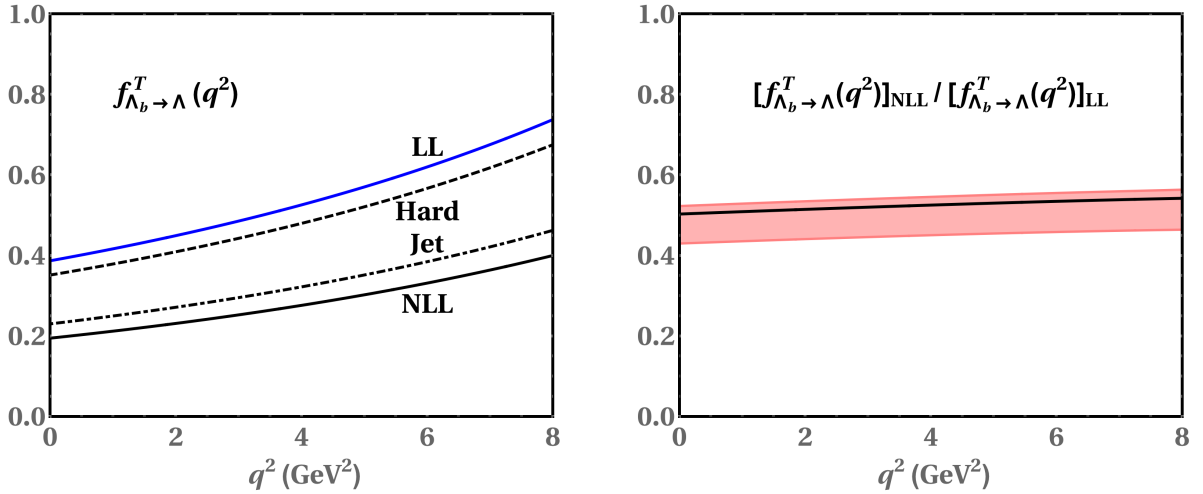


Figure 7: Breakdown of the one-loop contribution to the sum rules of  $f_{\Lambda_b \rightarrow \Lambda}^T(q^2)$  from the NLO hard and the NLO jet functions (left panel) and the momentum transfer dependence of the ratio  $[f_{\Lambda_b \rightarrow \Lambda}^T(q^2)]_{\text{NLL}} / [f_{\Lambda_b \rightarrow \Lambda}^T(q^2)]_{\text{LL}}$  with theory uncertainties from varying the renormalization and the factorization scales (right panel).

$\Lambda_b \rightarrow \Lambda$  form factors. It is evident that the sum rules of  $f_{\Lambda_b \rightarrow \Lambda}^T(0)$  exhibits extraordinary mild dependence on the Borel mass parameter due to a strong cancellation of the systematic uncertainty between the LCSR of  $f_{\Lambda_b \rightarrow \Lambda}^T(0)$  and the QCD sum rules of the coupling  $f_\Lambda$ . One can further find that both the leading-logarithmic (LL) and the NLL resummation improved sum rules are insensitive to the factorization scale  $\mu$  in the allowed interval and resummation of parametrically large logarithms in the hard matching coefficients only induces a minor impact on the sum rules for  $f_{\Lambda_b \rightarrow \Lambda}^T(0)$  numerically compared with the one-loop fixed-order correction. More importantly, the perturbative  $\mathcal{O}(\alpha_s)$  correction is found to reduce the tree-level sum rule prediction by a factor of 1/2, implying the importance of QCD radiative effect in baryonic sum rule applications (see also [54] for a similar observation on the perturbative spectral function of the vacuum-to-vacuum correlation function defined with two baryonic currents in HQET).

To develop a better understanding of the origin of the significant perturbative correction, we break the complete one-loop contribution to the sum rules of  $f_{\Lambda_b \rightarrow \Lambda}^T(0)$  down into the hard and the hard-collinear corrections, which are defined as replacing  $\psi_{4,\text{eff}}(\omega', \mu, \nu)$  in Eq. (113) by  $\tilde{\psi}_4(\omega')$  for the former and as replacing  $[U_1(\bar{n} \cdot p'/2, \mu_h, \mu) C_{\perp, V(A)}(n \cdot p', \mu_h)]$  by one for the latter. In Fig. 7 (left panel) we plot the separate perturbative contributions from hard and hard-collinear fluctuations as functions of the momentum transfer squared. We can readily find that the dominant  $\alpha_s$  correction at one loop is from the NLO jet (hard-collinear) function instead of the NLO hard function and this highlights the importance of the perturbative

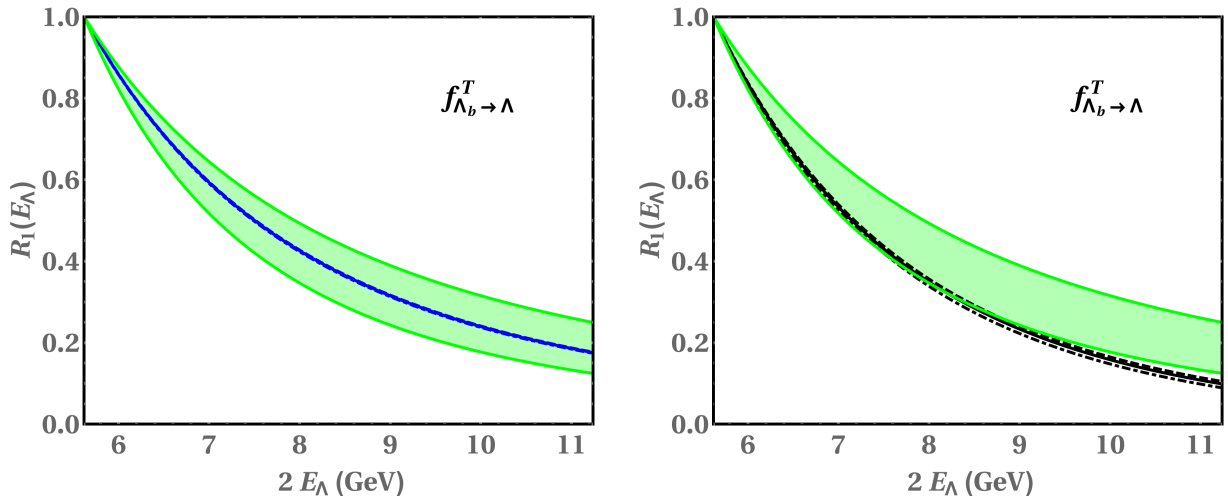


Figure 8: Dependence of the ratio  $R_1(E_\Lambda)$  on the  $\Lambda$ -baryon energy  $E_\Lambda$ . The blue (left panel) and the black (right panel) curves are obtained from the LL and NLL sum rule predictions, respectively. The two green curves refer to a pure  $1/E_\Lambda^2$  and a pure  $1/E_\Lambda^3$  dependence.

matching calculations at the hard-collinear scale performed in this paper. The  $q^2$ -dependence of the ratio  $[f_{\Lambda_b \rightarrow \Lambda}^T(q^2)]_{\text{NLL}} / [f_{\Lambda_b \rightarrow \Lambda}^T(q^2)]_{\text{LL}}$  with the theory uncertainty estimated from varying both the renormalization and the factorization scales in the acceptable ranges are displayed in the right panel of Fig. 7.

We now turn to investigate the  $\Lambda$ -baryon energy dependence of the form factor  $f_{\Lambda_b \rightarrow \Lambda}^T(q^2)$ , from the sum rules at LL and at NLL accuracy, which is of particular conceptual interest in that the soft overlap contributions and the hard-spectator scattering effects in the heavy-to-light baryonic form factors differ in the scaling of  $1/E_\Lambda$  at large hadronic recoil. For this purpose, we introduce the following ratio originally proposed in [10]

$$R_1(E_\Lambda) = \frac{f_{\Lambda_b \rightarrow \Lambda}^T(n \cdot p')}{f_{\Lambda_b \rightarrow \Lambda}^T(m_{\Lambda_b})}, \quad (130)$$

where we have switched the argument of the form factor from  $q^2$  as used in the remainder of this paper to  $n \cdot p' \simeq 2 E_\Lambda$ . As shown in Fig. 8, the predicted energy dependence of  $f_{\Lambda_b \rightarrow \Lambda}^T$  from the LL sum rules exhibits a scaling behaviour in between  $1/E_\Lambda^2$  and  $1/E_\Lambda^3$  for the default choices of theory input parameters, while the NLL sum rule prediction favors evidently a  $1/E_\Lambda^3$  behavior in consistent with the power counting analysis. We have also verified that such observation can be made for the energy dependence of all the other  $\Lambda_b \rightarrow \Lambda$  form factors.

Since the light-cone operator-product expansion of the correlation functions  $\Pi_{\mu,a}(p, q)$  can only be justified at low  $q^2$ , we need to extrapolate the sum rule predictions for the  $\Lambda_b \rightarrow \Lambda$  form

factors at  $q^2 \leq q_{\text{max}}^2 = 8 \text{ GeV}^2$  toward large momentum transfer  $q^2$ . To this end, we apply the simplified  $z$ -series parametrization [55] based upon the conformal mapping of the cut  $q^2$ -plane onto the disk  $|z(q^2, t_0)| \leq 1$  in the complex  $z$ -plane with the standard transformation

$$z(q^2, t_0) = \frac{\sqrt{t_+ - q^2} - \sqrt{t_+ - t_0}}{\sqrt{t_+ - q^2} + \sqrt{t_+ - t_0}}. \quad (131)$$

The parameter  $t_+$  is determined by the threshold of the lowest continuum state which can be excited by the weak transition current in QCD. It is evident that all the channels  $|BK\rangle$ ,  $|B_s\pi\rangle$  and  $|\Lambda_b\bar{\Lambda}\rangle$  can be produced by the  $\bar{s}\Gamma_{\mu,a}b$  current, the form factors can be analytical functions in the complex  $q^2$ -plane cut along the real axis for

$$q^2 \geq \min \{ (m_{B_s} + m_\pi)^2, (m_B + m_K)^2, (m_{\Lambda_b} + m_\Lambda)^2 \} = (m_{B_s} + m_\pi)^2, \quad (132)$$

in addition to the potential resonances below the branch cut. We theretofore need to set  $t_+ = (m_{B_s} + m_\pi)^2$  for all the  $\Lambda_b \rightarrow \Lambda$  form factors. The auxiliary parameter  $t_0$  determines the  $q^2$  point that will be mapped onto the origin of the complex  $z$ -plane, and in practice we will choose  $t_0 = (m_{\Lambda_b} - m_\Lambda)^2$  following [56]. Since the helicity form factors are constructed from the hadronic matrix elements of weak transition currents with definite spin-parity quantum numbers by projecting on the polarization vector for a spin-one particle with the four-momentum  $q_\mu$ , we collect some fundamental information of the lowest resonances produced by the helicity-projected weak currents in Table 1.

form factor	$B_s(J^P)$	Mass (GeV)	Ref.
$f_{\Lambda_b \rightarrow \Lambda}^{+,T}(q^2), h_{\Lambda_b \rightarrow \Lambda}^{+,T}(q^2)$	$B_s^*(1^-)$	5.42	[57]
$f_{\Lambda_b \rightarrow \Lambda}^0(q^2)$	$B_{s0}(0^+)$	5.72	(our estimate)
$g_{\Lambda_b \rightarrow \Lambda}^{+,T}(q^2), \tilde{h}_{\Lambda_b \rightarrow \Lambda}^{+,T}(q^2)$	$B_{s1}(1^+)$	5.83	[57]
$g_{\Lambda_b \rightarrow \Lambda}^0(q^2)$	$B_s(0^-)$	5.37	[57]

Table 1: Summary of the masses of low-lying resonances produced by the helicity-projected weak currents  $\bar{s}\Gamma_{\mu,a}b$  in QCD. Since the scalar  $B_{s0}$  meson has not been observed experimentally yet, we estimate its mass using an approximate SU(3) symmetry relation  $m_{B_{s0}} - m_{B_s} = m_{B_{d0}} - m_{B_d}$ , which is found to be comparable to that predicted by the heavy quark/chiral symmetry [58].

Since the lowest resonances of the scalar and the axial-vector channels are above the continuum threshold  $\sqrt{t_+}$ , it is therefore not necessary to introduce a pole factor in the  $z$ -series parameterizations of the corresponding form factors. Keeping the series expansion of the form factors to the first power of  $z$ -parameter we propose the following parameterizations

$$F_{\Lambda_b \rightarrow \Lambda}^{(I),i}(q^2) = \frac{F_{\Lambda_b \rightarrow \Lambda}^i(0)}{1 - q^2/m_{B_s^*}^2} \{1 + b_1^i [z(q^2, t_0) - z(0, t_0)]\} \quad (133)$$

for the form factors  $f_{\Lambda_b \rightarrow \Lambda}^{+,T}(q^2)$  and  $h_{\Lambda_b \rightarrow \Lambda}^{+,T}(q^2)$ ,

$$F_{\Lambda_b \rightarrow \Lambda}^{(II),i}(q^2) = \frac{F_{\Lambda_b \rightarrow \Lambda}^i(0)}{1 - q^2/m_{B_s}^2} \{1 + b_1^i [z(q^2, t_0) - z(0, t_0)]\} \quad (134)$$

for the form factor  $g_{\Lambda_b \rightarrow \Lambda}^0(q^2)$ , and

$$F_{\Lambda_b \rightarrow \Lambda}^{(III),i}(q^2) = F_{\Lambda_b \rightarrow \Lambda}^i(0) \{1 + b_1^i [z(q^2, t_0) - z(0, t_0)]\} \quad (135)$$

for the form factors  $f_{\Lambda_b \rightarrow \Lambda}^0(q^2)$ ,  $g_{\Lambda_b \rightarrow \Lambda}^{+,T}(q^2)$ , and  $\tilde{h}_{\Lambda_b \rightarrow \Lambda}^{+,T}(q^2)$ . The shape parameters  $b_1^i$  can be determined by matching the  $z$ -series parameterizations to the NLL sum rule predictions at large hadronic recoil, i.e.,  $0 \leq q^2 \leq q_{\text{max}}^2 = 8 \text{ GeV}^2$ . The resulting form factors in the allowed kinematical region  $0 \leq q^2 \leq t_0$  are displayed in Figs. 9 and 10, where independent calculations of these QCD form factors from Lattice determinations of the two HQET form factors at low hadronic recoil [21] are also presented for a comparison.

To facilitate such a comparison we first need to perform the perturbative matching of the heavy-to-light currents from QCD onto HQET [59]

$$\begin{aligned} \bar{s} \gamma_\mu (1, \gamma_5) b &= c_\gamma \bar{s} \gamma_\mu (1, \gamma_5) h + c_v \bar{s} v_\mu (1, -\gamma_5) b + \dots, \\ \bar{s} \sigma_{\mu\nu} (1, \gamma_5) b &= c_\sigma \bar{s} \sigma_{\mu\nu} (1, \gamma_5) h + \dots, \end{aligned} \quad (136)$$

at leading power in  $\Lambda/m_b$ , where the matching coefficients at one loop are given by

$$\begin{aligned} c_\gamma &= 1 - \frac{\alpha_s C_F}{4\pi} \left[ 3 \ln \frac{\mu}{m_b} + 4 \right] + \mathcal{O}(\alpha_s^2), \\ c_v &= \frac{\alpha_s C_F}{2\pi} + \mathcal{O}(\alpha_s^2), \\ c_\sigma &= 1 - \frac{\alpha_s C_F}{4\pi} \left[ 5 \ln \frac{\mu}{m_b} + 4 \right] + \mathcal{O}(\alpha_s^2). \end{aligned} \quad (137)$$

The HQET matrix element defined with an arbitrary Dirac structure of the leading-power effective current can be expressed by two Isgur-Wise functions at low hadronic recoil [59, 60]

$$\langle \Lambda(p', s') | \bar{s} \Gamma h | \Lambda_b(v, s) \rangle = \bar{\Lambda}(p', s') [F_1(v \cdot p') + F_2(v \cdot p') \not{v}] \Gamma \Lambda_b(v, s), \quad (138)$$

due to the heavy-quark spin symmetry. It is then straightforward to write

$$f_{\Lambda_b \rightarrow \Lambda}^T = c_\gamma (F_1 - F_2),$$

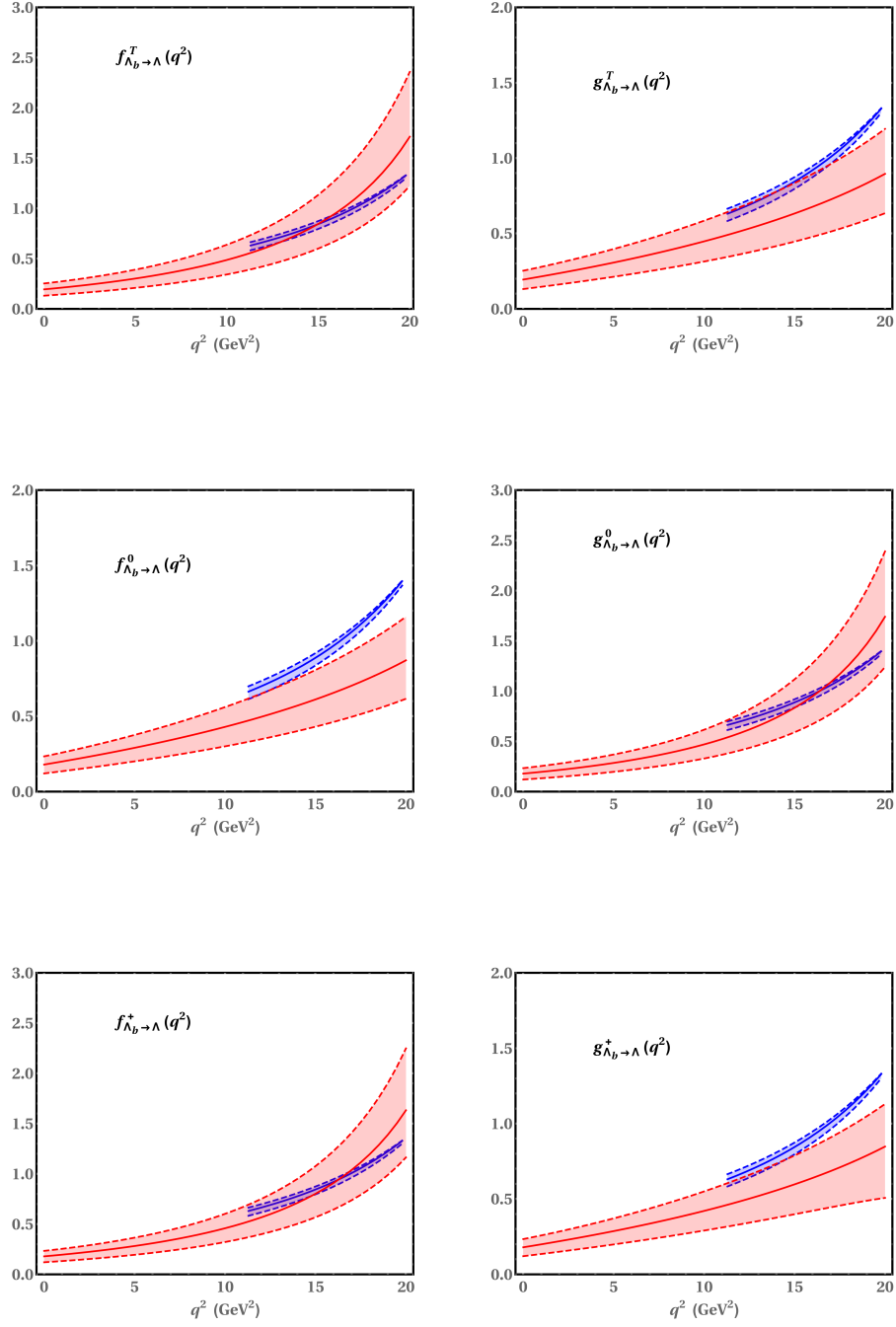


Figure 9: The  $\Lambda_b \rightarrow \Lambda$  form factors induced by the (axial)-vector currents computed from the LCSR approach at NLL accuracy and fitted to the  $z$ -series parameterizations. The pink (solid) and the blue (solid) curves refer to the predictions from the LCSR with an extrapolation and from the Lattice calculations [21], respectively, and the uncertainty bands are obtained by adding all separate theory uncertainties in quadrature.

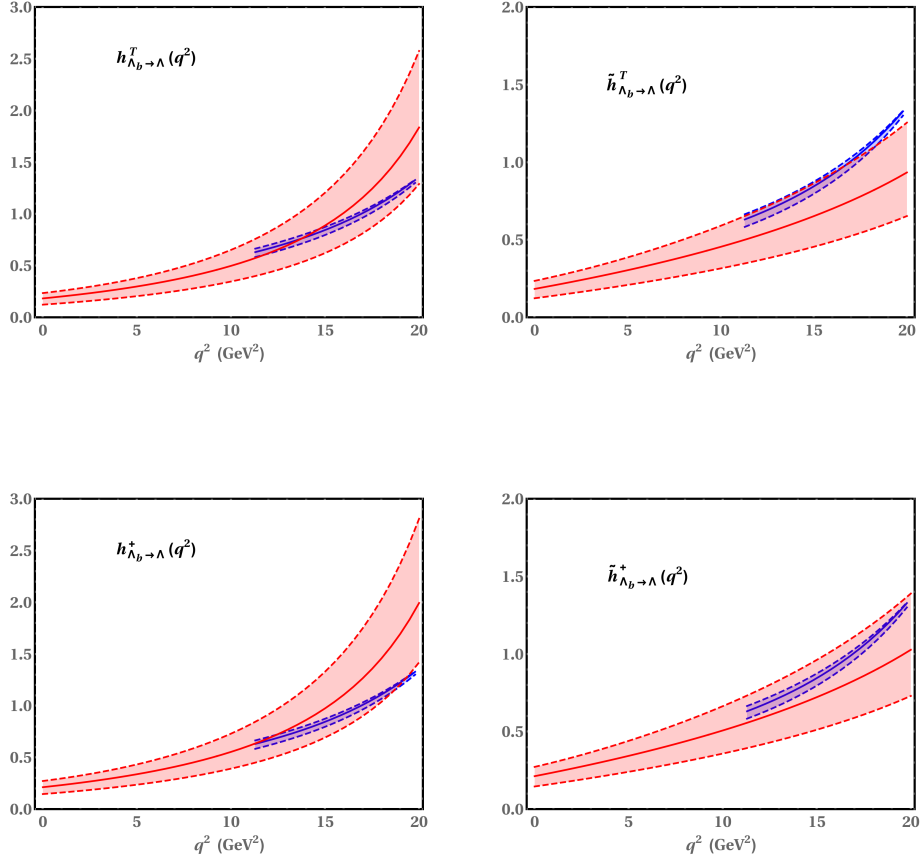


Figure 10: The  $\Lambda_b \rightarrow \Lambda$  form factors induced by the (pseudo)-tensor currents computed from the LCSR approach at NLL accuracy and fitted to the  $z$ -series parameterizations. Same conventions as in Fig. 9.

$$\begin{aligned}
f_{\Lambda_b \rightarrow \Lambda}^0 &= (c_\gamma + c_v) (F_1 + F_2) , \\
f_{\Lambda_b \rightarrow \Lambda}^+ &= c_\gamma (F_1 - F_2) , \\
g_{\Lambda_b \rightarrow \Lambda}^T &= c_\gamma (F_1 + F_2) , \\
g_{\Lambda_b \rightarrow \Lambda}^0 &= (c_\gamma + c_v) (F_1 - F_2) , \\
g_{\Lambda_b \rightarrow \Lambda}^+ &= c_\gamma (F_1 + F_2) , \\
h_{\Lambda_b \rightarrow \Lambda}^{+,T} &= c_\sigma (F_1 - F_2) , \\
\tilde{h}_{\Lambda_b \rightarrow \Lambda}^{+,T} &= c_\sigma (F_1 + F_2) ,
\end{aligned} \tag{139}$$

at low recoil. Inspection of Figs. 9 and 10 indicates that the LCSR calculations with the aid of an extrapolation inspired by the  $z$ -series expansion and the Lattice determinations in HQET reach a reasonable agreement in general at low hadronic recoil. However, the Lattice calculations [21], on the other hand, reveal faster growing form factors of  $f_{\Lambda_b \rightarrow \Lambda}^0$ ,  $g_{\Lambda_b \rightarrow \Lambda}^{+,T}$  and  $\tilde{h}_{\Lambda_b \rightarrow \Lambda}^{+,T}$  but slower increasing form factors of  $f_{\Lambda_b \rightarrow \Lambda}^{+,T}$ ,  $g_{\Lambda_b \rightarrow \Lambda}^0$  and  $h_{\Lambda_b \rightarrow \Lambda}^{+,T}$  at high momentum transfer squared when confronted with the LCSR-assisted  $z$ -parametrization predictions. The observed shape discrepancies might be attributed to the unaccounted power-enhanced but  $\alpha_s$ -suppressed hard scattering effects, and to the yet unknown higher order/power corrections, to the systematic uncertainties induced by the parton-hadronic quality approximation and truncations of the  $z$ -series expansion in our calculations, as well as to the power-suppressed contributions and to the uncounted systematic uncertainties in the Lattice determinations.

We now collect the calculated form factors at zero momentum transfer  $F_{\Lambda_b \rightarrow \Lambda}^i(0)$  and the fitted shape parameters  $b_1^i$  in Tables 2 and 3, where the numerically important uncertainties due to variations of the theory input parameters are also displayed.

Several comments on the numerical results obtained above are in order.

- The dominant theory uncertainty for the form factors at  $q^2 = 0$  computed from the NLL LCSR is due to the variation of the  $\omega_0$  parameter entering the  $\Lambda_b$ -baryon DA  $\phi_4(\omega, \mu_0)$ , while the most significant sources of the theory errors for the shape parameters  $b_1^i$  are from the different parameterizations of  $\phi_4(\omega, \mu_0)$  and from the variations of the renormalization scale  $\mu$  and of the factorization scale  $\nu$ .
- Large-recoil symmetry violation effects for the  $\Lambda_b \rightarrow \Lambda$  form factors are found to be relatively small, at the level of 20 %, albeit with the observed substantial perturbative QCD corrections to the form factors themselves. This can be readily understood from the fact that the NLO perturbative contributions to the  $\Lambda_b \rightarrow \Lambda$  form factors are dominated by the hard-collinear corrections which preserve the large-recoil symmetry in the heavy quark limit.
- Large discrepancies of the slope parameters are observed for the two form factors defined by the matrix elements of the two weak currents with the same helicity projections but with the opposite space-time parities, e.g.,  $f_{\Lambda_b \rightarrow \Lambda}^T$  and  $g_{\Lambda_b \rightarrow \Lambda}^T$ . This is in a nutshell due to the distinct analytical structures of two types of form factors below the branch cut in

Parameter	Central value	$\phi_4(\omega)$	$\omega_0$	$\{\mu, \nu\}$	$\{\mu_h, \nu'\}$	$M^2$	$s_0$
$f_{\Lambda_b \rightarrow \Lambda}^T(0)$	0.20	—	-0.04 +0.04	-0.03 -0.02	+0.02 -0.01	+0.01 -0.01	+0.00 -0.00
$b_1^{f_{\Lambda_b \rightarrow \Lambda}^T}$	-6.82	-2.93 -1.87	-1.16 +1.02	+0.12 +2.22	-0.30 +0.48	+0.22 -0.34	+0.25 -0.28
$b_1^{g_{\Lambda_b \rightarrow \Lambda}^T}$	-13.66	-3.72 -2.36	-1.46 +1.30	+0.15 -2.81	-0.38 +0.61	+0.28 -0.42	+0.32 -0.35
$f_{\Lambda_b \rightarrow \Lambda}^0(0)$	0.18	—	-0.04 +0.04	-0.03 +0.02	+0.02 -0.01	+0.01 -0.01	+0.00 -0.00
$b_1^{f_{\Lambda_b \rightarrow \Lambda}^0}$	-14.59	-3.91 -2.51	-1.61 +1.40	+0.11 -3.51	-0.36 +0.60	+0.33 -0.51	+0.35 -0.40
$b_1^{g_{\Lambda_b \rightarrow \Lambda}^0}$	-7.43	-3.06 -1.97	-1.26 +1.11	+0.10 -2.75	-0.28 +0.48	+0.26 -0.40	+0.28 -0.31
$f_{\Lambda_b \rightarrow \Lambda}^+(0)$	0.18	—	-0.04 +0.04	-0.03 -0.02	+0.02 -0.01	+0.01 -0.01	+0.00 -0.00
$b_1^{f_{\Lambda_b \rightarrow \Lambda}^+}$	-7.17	-3.07 -1.97	-1.24 +1.09	+0.09 -2.53	-0.29 +0.49	+0.25 -0.38	+0.28 -0.31
$b_1^{g_{\Lambda_b \rightarrow \Lambda}^+}$	-14.10	-3.88 -2.48	-1.56 +1.38	+0.11 -3.19	-0.36 +0.62	+0.32 -0.47	+0.35 -0.38

Table 2: Summary of the calculated form factors induced by the (axial)-vector weak transition currents at  $q^2 = 0$  and the fitted shape parameters  $b_1^i$  with the uncertainties from the variations of various input parameters.



Parameter	Central value	$\phi_4(\omega)$	$\omega_0$	$\{\mu, \nu\}$	$\{\mu_h, \nu'\}$	$M^2$	$s_0$
$h_{\Lambda_b \rightarrow \Lambda}^T(0)$	0.18	—	-0.04 +0.04	-0.03 -0.01	+0.00 +0.01	+0.01 -0.01	+0.00 -0.00
$b_1^{h_{\Lambda_b \rightarrow \Lambda}^T}$	-8.26	-3.08 -1.99	-1.31 +1.14	+0.53 -3.52	-0.60 +0.76	+0.28 -0.44	+0.29 -0.33
$b_1^{\tilde{h}_{\Lambda_b \rightarrow \Lambda}^T}$	-15.49	-3.90 -2.52	-1.66 +1.45	+0.67 -4.45	-0.76 +0.97	+0.36 -0.56	+0.37 -0.41
$h_{\Lambda_b \rightarrow \Lambda}^+(0)$	0.21	—	-0.05 +0.05	-0.00 -0.00	+0.00 +0.01	+0.01 -0.01	+0.00 -0.00
$b_1^{h_{\Lambda_b \rightarrow \Lambda}^+}$	-7.51	-2.84 -1.81	-1.15 +1.03	+0.52 -2.81	-0.50 +0.66	+0.23 -0.35	+0.26 -0.28
$b_1^{\tilde{h}_{\Lambda_b \rightarrow \Lambda}^+}$	-14.53	-3.61 -2.29	-1.46 +1.30	+0.65 -3.57	-0.64 +0.84	+0.29 -0.45	+0.32 -0.36

Table 3: Summary of the calculated form factors induced by the (pseudo)-tensor weak transition currents at  $q^2 = 0$  and the fitted shape parameters  $b_1^i$  with the uncertainties from the variations of various input parameters.

the complex- $q^2$  plane which lead to the different  $z$ -series parameterizations adopted in the fitting programmes.

## 6 Phenomenological applications

In this section we aim at exploring phenomenological applications of the calculated  $\Lambda_b \rightarrow \Lambda$  form factors which serve as fundamental ingredients for the theory description of the electro-weak penguin induced  $\Lambda_b \rightarrow \Lambda \ell^+ \ell^-$  decays. QCD dynamics of the hadronic  $\Lambda_b \rightarrow \Lambda \ell^+ \ell^-$  decay amplitude is, however, more complicated due to the non-factorizable strong interaction effects which arise from QED corrections to the matrix elements of the four-quark operators and the gluonic penguin operator in the weak effective Hamiltonian. Some typical non-factorizable contributions to the  $\Lambda_b \rightarrow \Lambda \ell^+ \ell^-$  matrix elements at  $\mathcal{O}(\alpha_s)$  are presented in Fig. 11, in analogy to the counterpart  $B \rightarrow K^* \ell^+ \ell^-$  decays discussed in [11]. It is evident that the spectator interaction effects displayed in the diagrams (b) and (d) and the weak annihilation contributions shown in (e) and (f) cannot be computed with QCD factorization formalism described in [11] and some non-perturbative QCD approaches are in demand to deal with such non-local hadronic matrix elements. We will restrict ourselves to the factorizable contributions to the  $\Lambda_b \rightarrow \Lambda \ell^+ \ell^-$  decay amplitude, at  $\mathcal{O}(\alpha_s^0)$ , in this work, and leave a systematic treatment of the non-form-factor corrections for a future work.

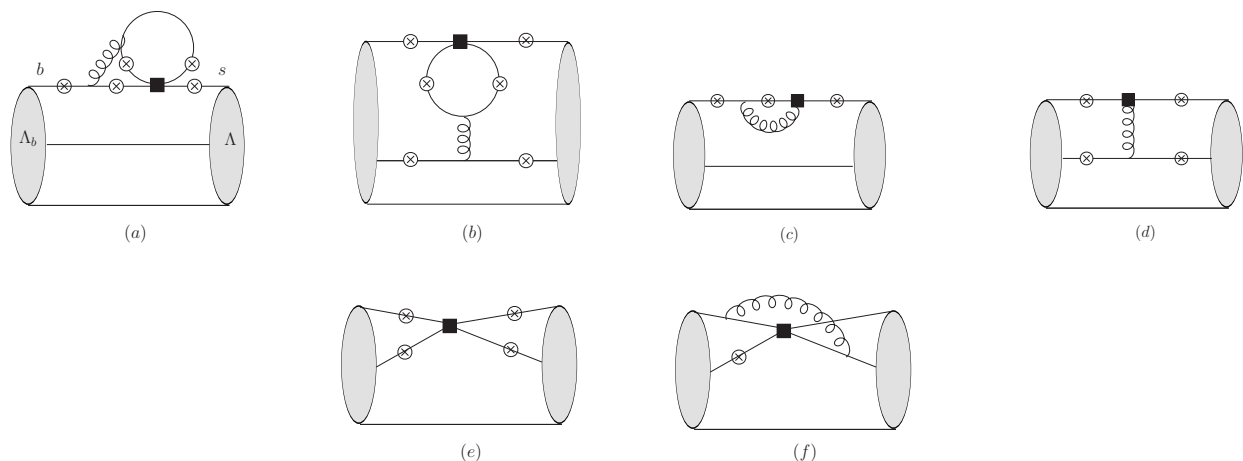


Figure 11: Various non-factorizable diagrams contributed to the  $\Lambda_b \rightarrow \Lambda \ell^+ \ell^-$  decays. The crossed circles indicate possible insertions of the virtual photon line and the black squares stand for the hadronic operator vertices. Taken from [61].

The double differential decay distribution of  $\Lambda_b \rightarrow \Lambda \ell^+ \ell^-$  in terms of the momentum transfer squared  $q^2$  and the angle  $\theta$  between the positively charged lepton and the  $\Lambda$ -baryon in the rest frame of the lepton pair is given by [2]

$$\frac{d\Gamma(\Lambda_b \rightarrow \Lambda \ell^+ \ell^-)}{dq^2 d\cos\theta} = \frac{3}{8} [H_T(q^2) (1 + \cos^2\theta) + 2H_A(q^2) \cos\theta + 2H_L(q^2) (1 - \cos^2\theta)], \quad (140)$$

where in the factorization limit the helicity amplitudes can be computed as

$$\begin{aligned}
H_T(q^2) = \mathcal{N} q^2 \frac{\lambda^{1/2}(m_{\Lambda_b}^2, m_{\Lambda}^2, q^2)}{96 \pi^3 m_{\Lambda_b}^3} \\
\left[ s_- \left( \left| C_9^{\text{eff}}(q^2) f_{\Lambda_b \rightarrow \Lambda}^T + \frac{2 m_{\Lambda_b} (m_{\Lambda_b} + m_{\Lambda})}{q^2} C_7^{\text{eff}} h_{\Lambda_b \rightarrow \Lambda}^T \right|^2 + |C_{10} f_{\Lambda_b \rightarrow \Lambda}^T|^2 \right) \right. \\
\left. + s_+ \left( \left| C_9^{\text{eff}}(q^2) g_{\Lambda_b \rightarrow \Lambda}^T + \frac{2 m_{\Lambda_b} (m_{\Lambda_b} - m_{\Lambda})}{q^2} C_7^{\text{eff}} \tilde{h}_{\Lambda_b \rightarrow \Lambda}^T \right|^2 + |C_{10} g_{\Lambda_b \rightarrow \Lambda}^T|^2 \right) \right], \quad (141)
\end{aligned}$$

$$\begin{aligned}
H_A(q^2) = -\mathcal{N} q^2 \frac{\lambda(m_{\Lambda_b}^2, m_{\Lambda}^2, q^2)}{48 \pi^3 m_{\Lambda_b}^3} \\
\text{Re} \left[ \left( C_9^{\text{eff}}(q^2) f_{\Lambda_b \rightarrow \Lambda}^T + \frac{2 m_{\Lambda_b} (m_{\Lambda_b} + m_{\Lambda})}{q^2} C_7^{\text{eff}} h_{\Lambda_b \rightarrow \Lambda}^T \right)^* (C_{10} g_{\Lambda_b \rightarrow \Lambda}^T) \right. \\
\left. + \left( C_9^{\text{eff}}(q^2) g_{\Lambda_b \rightarrow \Lambda}^T + \frac{2 m_{\Lambda_b} (m_{\Lambda_b} - m_{\Lambda})}{q^2} C_7^{\text{eff}} \tilde{h}_{\Lambda_b \rightarrow \Lambda}^T \right)^* (C_{10} f_{\Lambda_b \rightarrow \Lambda}^T) \right], \quad (142)
\end{aligned}$$

$$\begin{aligned}
H_L(q^2) = \mathcal{N} \frac{\lambda^{1/2}(m_{\Lambda_b}^2, m_{\Lambda}^2, q^2)}{192 \pi^3 m_{\Lambda_b}^3} \\
\left[ s_- (m_{\Lambda_b} + m_{\Lambda})^2 \left( \left| C_9^{\text{eff}}(q^2) f_{\Lambda_b \rightarrow \Lambda}^+ + \frac{2 m_{\Lambda_b}}{m_{\Lambda_b} + m_{\Lambda}} C_7^{\text{eff}} h_{\Lambda_b \rightarrow \Lambda}^+ \right|^2 + |C_{10} f_{\Lambda_b \rightarrow \Lambda}^+|^2 \right) \right. \\
\left. + s_+ (m_{\Lambda_b} - m_{\Lambda})^2 \left( \left| C_9^{\text{eff}}(q^2) g_{\Lambda_b \rightarrow \Lambda}^+ + \frac{2 m_{\Lambda_b}}{m_{\Lambda_b} - m_{\Lambda}} C_7^{\text{eff}} \tilde{h}_{\Lambda_b \rightarrow \Lambda}^+ \right|^2 + |C_{10} g_{\Lambda_b \rightarrow \Lambda}^+|^2 \right) \right], \quad (143)
\end{aligned}$$

with

$$\mathcal{N} = \frac{G_F^2 \alpha_{em}^2}{8 \pi^2} |V_{ts} V_{tb}|^2, \quad \lambda(a, b, c) = a^2 + b^2 + c^2 - 2ab - 2ac - 2bc. \quad (144)$$

The detailed expressions for the effective Wilson coefficients  $C_9^{\text{eff}}(q^2)$  and  $C_7^{\text{eff}}$  in the NDR scheme with anti-commuting  $\gamma_5$  can be found in [11].

Evaluating the helicity amplitudes with the form factors computed from the NLL LCSR obtained in the above yields the differential branching fraction of  $\Lambda_b \rightarrow \Lambda \ell^+ \ell^-$  as a function of  $q^2$  plotted in Fig. 12 and the partially integrated decay rate over the  $q^2$  intervals from [44] displayed in Table 4. The theory predictions are also confronted with the experimental measurements from CDF [62] and LHCb [44]. The LHCb data except for the first  $q^2$ -bin are found to be systematically lower than the theory predictions at large hadronic recoil, while the sizeable uncertainties of the CDF measurements prevent us from drawing a definite conclusion.

Following [44] we further consider the forward-backward asymmetry and the longitudinal polarization fraction of the di-lepton system

$$A_{\text{FB}}(q^2) = \frac{\int_0^1 d \cos \theta \frac{d\Gamma(\Lambda_b \rightarrow \Lambda \ell^+ \ell^-)}{dq^2 d \cos \theta} - \int_{-1}^0 d \cos \theta \frac{d\Gamma(\Lambda_b \rightarrow \Lambda \ell^+ \ell^-)}{dq^2 d \cos \theta}}{d\Gamma(\Lambda_b \rightarrow \Lambda \ell^+ \ell^-)/dq^2},$$

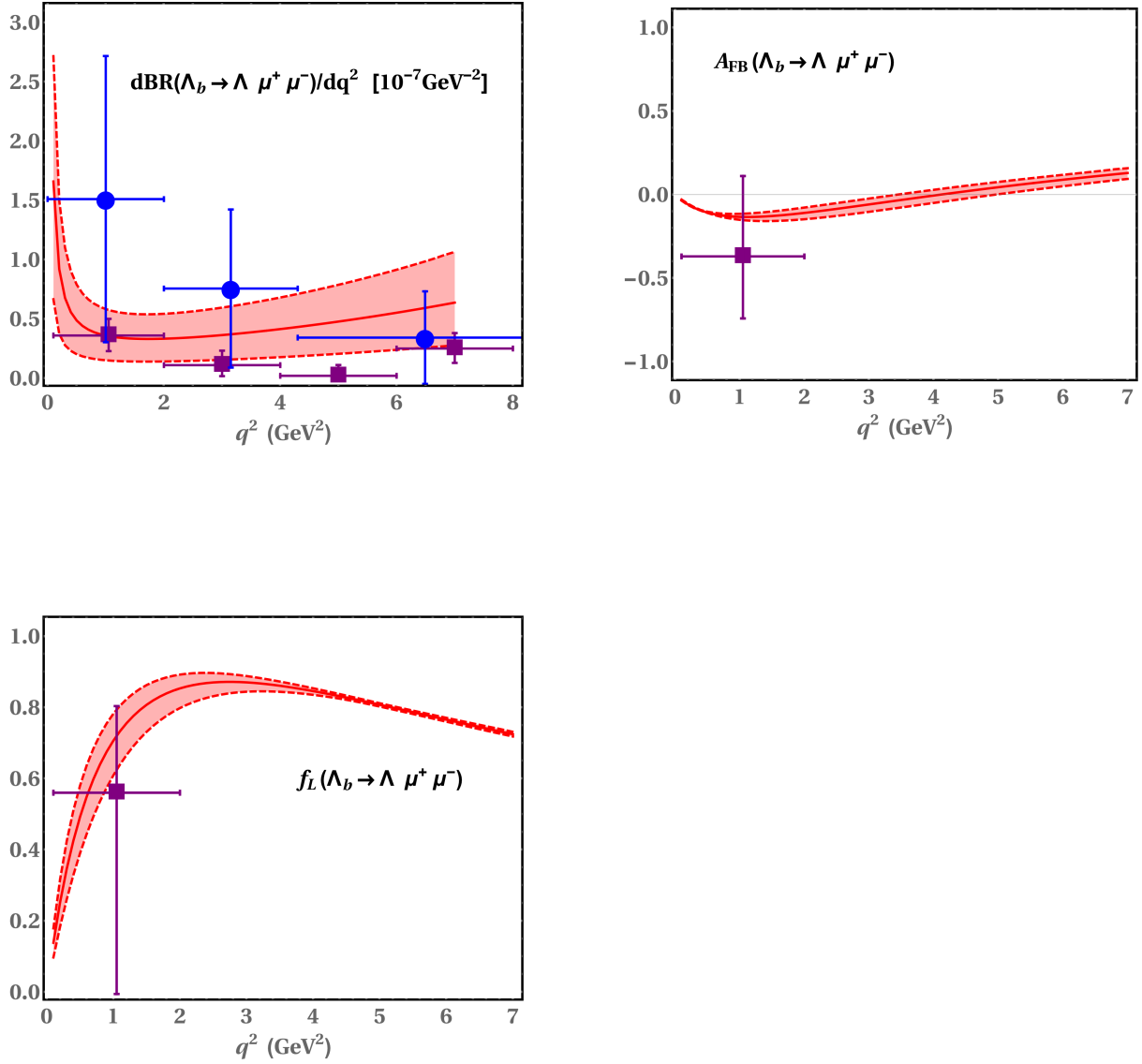


Figure 12: The differential branching fraction, the leptonic forward-backward asymmetry and the longitudinal polarization fraction of the di-lepton system for  $\Lambda_b \rightarrow \Lambda \ell^+ \ell^-$  as functions of  $q^2$  in the factorization limit. The solid (pink) curve corresponds to the NLL sum rule predictions with the central input and the shaded region (pink) indicates the theory uncertainties from the calculated form factors. The experimental data bins are taken from LHCb [44] (purple squares) and CDF [62] (blue full circles).

$$f_L(q^2) = \frac{H_L(q^2)}{H_L(q^2) + H_T(q^2)}, \quad (145)$$

where the definition of  $A_{\text{FB}}(q^2)$  differs from [44] due to the distinct convention of the  $\theta$  angle. We plot the  $q^2$  dependence of the differential forward-backward asymmetry and the longitudinal polarization fraction in Fig. 12, and collect the theory predictions for the binned distributions of these two observables in Table 4.

$[q_{\text{min}}^2, q_{\text{max}}^2]$ (GeV <sup>2</sup> )	$d\text{BR}/dq^2$ (10 <sup>-7</sup> GeV <sup>-2</sup> )		$A_{\text{FB}}$		$f_L$	
	this work	LHCb	this work	LHCb	this work	LHCb
[0.1, 2.0]	$0.45^{+0.28}_{-0.26}$	$0.36^{+0.14}_{-0.13}$	$-0.10^{+0.01}_{-0.01}$	$-0.37^{+0.48}_{-0.37}$	$0.57^{+0.08}_{-0.10}$	$0.56^{+0.24}_{-0.57}$
[2.0, 4.0]	$0.37^{+0.23}_{-0.21}$	$0.11^{+0.12}_{-0.09}$	$-0.06^{+0.04}_{-0.04}$	—	$0.86^{+0.02}_{-0.03}$	—
[4.0, 6.0]	$0.48^{+0.31}_{-0.27}$	$0.02^{+0.09}_{-0.01}$	$0.05^{+0.03}_{-0.04}$	—	$0.80^{+0.00}_{-0.00}$	—
[1.1, 6.0]	$0.41^{+0.26}_{-0.23}$	$0.09^{+0.06}_{-0.05}$	$-0.02^{+0.03}_{-0.04}$	—	$0.83^{+0.02}_{-0.02}$	—

Table 4: Summary of the theory predictions for the binned distributions of the branching fraction, the forward-backward asymmetry and the longitudinal polarization fraction. We also present the experimental data bins from LHCb [44] for a comparison, where various experimental uncertainties are added in quadrature.

Several comments on the numerical results computed in the above are in order.

- In contrast to the  $B \rightarrow K^* \ell^+ \ell^-$  decays, the theory uncertainty of the leptonic forward-backward asymmetry at the zero crossing point is not reduced compared to that at a different value of  $q^2$ . This can be readily understood from the fact that  $A_{\text{FB}}$  is not an optimized observable which is insensitive to the soft form factors in the former case, while it becomes an optimized observable in the latter case due to a single soft form factor governing the strong interaction dynamics of the  $\Lambda_b \rightarrow \Lambda$  form factors in the SCET limit. The location of the zero-crossing point of  $A_{\text{FB}}$  is determined as

$$q_0^2 = 4.1^{+0.9}_{-0.7} \text{ GeV}^2.$$

- The uncertainty band of the longitudinal polarization fraction  $f_L(q^2)$  shown in Fig. 12 indicates rather interesting features of the different dominant mechanisms contributing

to  $f_L(q^2)$  at different momentum transfer. At very large hadronic recoil  $q^2 \ll 1 \text{ GeV}^2$  the longitudinal helicity amplitude  $H_L$  is strongly suppressed compared to the transverse amplitude  $H_T$  which receives a large contribution from the photon pole. This indicates that  $f_L(q^2)$  at very large recoil receives a suppression factor of  $q^2/m_{\Lambda_b}^2$  and the resulting theory uncertainty is also negligible. In the vicinity of the zero-crossing point of  $A_{\text{FB}}$ , both helicity amplitudes  $H_L$  and  $H_T$  will be dominated by the contribution from the semileptonic operator  $O_{10}$ . The longitudinal polarization fraction  $f_L(q^2)$  is then, to a large extent, determined by a unique form-factor ratio  $f_{\Lambda_b \rightarrow \Lambda}^+(q^2)/f_{\Lambda_b \rightarrow \Lambda}^T(q^2)$  which suffers from a much smaller theory uncertainty compared to the other two ratios  $h_{\Lambda_b \rightarrow \Lambda}^T(q^2)/f_{\Lambda_b \rightarrow \Lambda}^T(q^2)$  and  $h_{\Lambda_b \rightarrow \Lambda}^+(q^2)/f_{\Lambda_b \rightarrow \Lambda}^T(q^2)$  that will also play an essential role in determining the value of  $f_L(q^2)$  for general momentum transfer. The most significant uncertainty of the latter two ratios is induced by the variation of the renormalization and the factorization scales. Based upon the above discussion, we conclude that the theory prediction of  $f_L(q^2)$  will involve a sizeable uncertainty only in the region  $1 \text{ GeV}^2 < q^2 < q_0^2$  displayed in Fig. 12.

- The theory prediction of the differential  $q^2$  distribution shown in Fig. 12 involves a large uncertainty due to the sensitivity to the  $\Lambda_b \rightarrow \Lambda$  form factors. To reduce the most important theory uncertainty from the poorly known shape parameter  $\omega_0$  in the  $\Lambda_b$ -baryon DA  $\phi_4(\omega, \mu_0)$ , one can introduce an optimized observable, the normalized differential  $q^2$  distribution, in analogy to that in  $B \rightarrow \pi \ell \nu$  [12]. It is however not the main objective of this work to explore the rich phenomenology encoded in the angular distributions of  $\Lambda_b \rightarrow \Lambda \ell^+ \ell^-$  emphasizing on the implications of optimized observables for new physics hunting.

## 7 Concluding discussion

In this paper we have performed, for this first time, perturbative QCD corrections to the  $\Lambda_b \rightarrow \Lambda$  form factors from the LCSR with the  $\Lambda_b$ -baryon DA at NLL accuracy. Applying the method of regions we have extracted both the hard coefficients and the jet functions entering the factorization formulae for the vacuum-to- $\Lambda_b$ -baryon correlation functions at one loop. In particular, we have verified a complete cancellation of the factorization-scale dependence for the factorized expressions of the considered correlation functions by computing the one-loop corrections to the  $\Lambda_b$ -baryon DA in QCD manifestly. Also, we demonstrated at the diagrammatic level that QCD factorization of the vacuum-to- $\Lambda_b$ -baryon correction functions with an arbitrary weak vertex can only depend on a universal jet function at leading power in  $\Lambda/m_b$ . Employing the RG evolution equations in momentum space and distinguishing the renormalization and the factorization scales, we further achieved the NLL resummation improved factorization formulae for the correlation functions defined with both the (axial)-vector and the (pseudo)-tensor weak currents. Making use of the parton-hadron duality approximation and implementing the continuum subtraction, we further obtained the NLL QCD sum rules of the  $\Lambda_b \rightarrow \Lambda$  form factors at large hadronic recoil. Since we concentrate on factorization of the correlation functions at leading power in  $\Lambda/m_b$ , we do not take into account the numerically insignificant contribution corresponding to the matrix element of the “ $B$ -type” SCET current, which can be computed with LCSR constructed from the same correlation functions

at sub-leading power or from the correlation functions with the “wrong” light-cone projector acting on the interpolating current of the  $\Lambda$ -baryon [2].

Proceeding with the obtained NLL sum rules on the light cone, we carried out an exploratory numerical analysis of the  $\Lambda_b \rightarrow \Lambda$  form factors, putting an emphasis on the various sources of perturbative and systematic uncertainties. To gain a better control of the shape parameter  $\omega_0$  for the  $\Lambda_b$ -baryon DA  $\phi_4(\omega, \mu_0)$ , the prediction of  $\Lambda_b \rightarrow p$  form factor  $f_{\Lambda_b \rightarrow p}^+(0)$  from the LCSR with the nucleon DA and the SU(3) flavour symmetry relation were taken as theory input in the matching determination of  $\omega_0$ . In analogy to the  $B \rightarrow \pi$  form factors, the sum rules of  $\Lambda_b \rightarrow \Lambda$  form factors are not only sensitive to the shape parameter  $\omega_0$  but also to the specific behavior of  $\phi_4(\omega, \mu_0)$  at small  $\omega$ . Of particular phenomenological interest are that the perturbative  $\mathcal{O}(\alpha_s)$  corrections result in a significant ( $\sim 50\%$ ) reduction of the tree-level sum rule predictions and the dominant one-loop correction is from the NLO jet function instead of the NLO hard functions entering the sum rules of the  $\Lambda_b \rightarrow \Lambda$  form factors. Such observations evidently highlight the importance of the perturbative matching calculation at the hard-collinear scale as accomplished in this work. Employing the  $z$ -series expansion, we extrapolated the LCSR predictions of the form factors toward large momentum transfer where our predictions are already confronted with the Lattice determinations of two HQET form factors. Expressing the QCD transition form factors in terms of the Isgur-Wise functions at low hadronic recoil, we observed a reasonable agreement for the predicted form factors at large momentum transfer between two independent calculations, albeit with the perceivable discrepancies on the  $q^2$  shapes of the  $\Lambda_b \rightarrow \Lambda$  form factors. In addition, the large-energy symmetry breaking effects for the form factors were found to be relatively small at one loop, since the NLO QCD corrections to the sum rules are dominated by the hard-collinear corrections preserving the symmetry relations.

Having at our disposal the theory predictions for the  $\Lambda_b \rightarrow \Lambda$  form factors, we investigated their phenomenological applications to the electro-weak penguin decays  $\Lambda_b \rightarrow \Lambda \ell^+ \ell^-$  in the factorization limit. The calculated differential  $q^2$  distribution in  $\Lambda_b \rightarrow \Lambda \ell^+ \ell^-$  turned out to be systematically lower than the LHCb measurements, except for the first data bin. We further computed the forward-backward asymmetry and the longitudinal polarization fraction for the di-lepton system which are comparable to the LHCb data for the lowest  $q^2$  bin. The longitudinal polarization fraction  $f_L(q^2)$  was found to be of particular phenomenological interest due to a large cancellation of the theory uncertainties for the  $\Lambda_b \rightarrow \Lambda$  form factors.

The heavy-to-light baryonic form factors are apparently not sufficient to provide a complete description of the strong interaction dynamics involved in  $\Lambda_b \rightarrow \Lambda \ell^+ \ell^-$  due to the non-factorizable contributions induced by the QED corrections to the matrix elements of hadronic operators in the weak Hamiltonian. The techniques developed in this work can be readily applied to evaluate the non-form-factor effects induced by the hard spectator interaction and the weak annihilation as displayed in Fig. 11. Since both the factorizable and the non-factorizable contributions to the  $\Lambda_b \rightarrow \Lambda \ell^+ \ell^-$  decay amplitude will be parameterized by the  $\Lambda_b$ -baryon DA without introducing any additional non-perturbative quantities, we are expected to have more opportunities to construct optimized observables insensitive to the hadronic uncertainties, provided that the systematic uncertainty of the sum rule approach is also cancelled to a large extent for these observables. We postpone a systematic treatment of such non-factorizable contribution as well as a detailed discussion of the angular observables

in  $\Lambda_b \rightarrow \Lambda \ell^+ \ell^-$  for a future work.

The strategies of computing the heavy-to-light baryonic form factors at  $\mathcal{O}(\alpha_s)$  presented here can be further extend to study the topical  $\Lambda_b \rightarrow p \ell \nu$  decays [63], which provide an alternative approach to determine the CKM matrix element  $|V_{ub}|$ . To this end, a comprehensive analysis of the evolution equations for all the DA defined in Eqs. (25) and (26) at one loop are in demand, since the spin structure of the light di-quark system in the  $\Lambda_b$ -baryon is distorted in the decay product, i.e., the nucleon. In this respect, the techniques developed in [20] based upon the spinor formalism and the conformal symmetry can be applied to facilitate the construction of the renormalization kernels in coordinate space. To summarize, we believe that the present work serves as an essential step towards understanding the strong interaction dynamics in various exclusive  $\Lambda_b$ -baryon decays and interesting extensions of the present calculations into different directions are expected, especially under the encouragement of the considerable progress on the beauty baryon decays from the experimental side.

## Acknowledgements

This work has been supported in part by the Gottfried Wilhelm Leibniz programme of the Deutsche Forschungsgemeinschaft (DFG).

## A Spectral representations

In this appendix we will collect the dispersion representations of convolution integrals appeared in the NLL resummation improved factorization formulae shown in (110), (111) and (112). As already mentioned in section 4, the spectral representations derived in the following are reduced with the assumption that  $\psi_4(\omega_1, \omega_2, \mu_0)$  only depends on the sum of two momentum variables  $\omega = \omega_1 + \omega_2$  as inspired from [2, 14, 18].

$$\begin{aligned}
& \frac{1}{\pi} \text{Im}_{\omega'} \int_0^\infty d\omega_1 \int_0^\infty d\omega_2 \frac{1}{\omega - \omega' - i0} \ln^2 \frac{\mu^2}{n \cdot p' (\omega - \omega')} \psi_4(\omega_1, \omega_2, \mu) \\
&= \int_0^{\omega'} d\omega \left[ \frac{2}{\omega - \omega'} \ln \frac{\mu^2}{n \cdot p' (\omega' - \omega)} \right]_{\oplus} \tilde{\psi}_4(\omega, \mu) + \left[ \ln^2 \frac{\mu^2}{n \cdot p' \omega'} - \frac{\pi^2}{3} \right] \tilde{\psi}_4(\omega', \mu), \quad (146) \\
& \frac{1}{\pi} \text{Im}_{\omega'} \int_0^\infty d\omega_1 \int_0^\infty d\omega_2 \frac{1}{\omega - \omega' - i0} \ln \frac{\omega - \omega'}{\omega_2 - \omega'} \ln \frac{\mu^2}{n \cdot p' (\omega - \omega')} \psi_4(\omega_1, \omega_2, \mu) \\
&= \omega' \int_0^{\omega'} d\omega \left[ \frac{1}{\omega - \omega'} \ln \frac{\omega' - \omega}{\omega'} \right]_{\oplus} \phi_4(\omega, \mu) + \int_0^{\omega'} d\omega \ln \frac{\mu^2}{n \cdot p' (\omega' - \omega)} \frac{d\tilde{\psi}_4(\omega, \mu)}{d\omega} \\
& \quad + \frac{\omega'}{2} \int_{\omega'}^\infty d\omega \left[ \ln^2 \frac{\mu^2}{n \cdot p' (\omega - \omega')} - \ln \frac{\mu^2}{n \cdot p' \omega'} + \frac{\pi^2}{3} \right] \frac{d\phi_4(\omega, \mu)}{d\omega}, \quad (147) \\
& \frac{1}{\pi} \text{Im}_{\omega'} \int_0^\infty d\omega_1 \int_0^\infty d\omega_2 \frac{1}{\omega - \omega' - i0} \ln^2 \frac{\omega - \omega'}{\omega_2 - \omega'} \psi_4(\omega_1, \omega_2, \mu)
\end{aligned}$$



$$= -\omega' \int_{\omega'}^{\infty} d\omega \left[ \ln^2 \frac{\omega - \omega'}{\omega'} + 2 \ln \frac{\omega - \omega'}{\omega'} - \frac{\pi^2}{3} + 2 \right] \frac{d\phi_4(\omega, \mu)}{d\omega}, \quad (148)$$

$$\begin{aligned} & \frac{1}{\pi} \text{Im}_{\omega'} \int_0^{\infty} d\omega_1 \int_0^{\infty} d\omega_2 \frac{1}{\omega - \omega' - i0} \frac{\omega_2 - \omega'}{\omega_1} \ln \frac{\omega - \omega'}{\omega_2 - \omega'} \psi_4(\omega_1, \omega_2, \mu) \\ &= \int_{\omega'}^{\infty} d\omega \left[ \ln \frac{\omega}{\omega - \omega'} + \omega' \left( \ln \frac{\omega - \omega'}{\omega'} + 1 \right) \frac{d}{d\omega} \right] \phi_4(\omega, \mu), \end{aligned} \quad (149)$$

$$\begin{aligned} & \frac{1}{\pi} \text{Im}_{\omega'} \int_0^{\infty} d\omega_1 \int_0^{\infty} d\omega_2 \frac{1}{\omega - \omega' - i0} \ln \frac{\omega - \omega'}{\omega_2 - \omega'} \psi_4(\omega_1, \omega_2, \mu) \\ &= -\omega' \int_{\omega'}^{\infty} d\omega \left[ \ln \frac{\omega - \omega'}{\omega'} + 1 \right] \frac{d\phi_4(\omega, \mu)}{d\omega}, \end{aligned} \quad (150)$$

$$\begin{aligned} & \frac{1}{\pi} \text{Im}_{\omega'} \int_0^{\infty} d\omega_1 \int_0^{\infty} d\omega_2 \frac{1}{\omega - \omega' - i0} \ln \frac{\mu^2}{n \cdot p' (\omega - \omega')} \psi_4(\omega_1, \omega_2) \\ &= \int_0^{\omega'} d\omega \ln \frac{\mu^2}{n \cdot p' (\omega' - \omega)} \frac{d\tilde{\psi}_4(\omega, \mu)}{d\omega}, \end{aligned} \quad (151)$$

where we have defined

$$\phi_4(\omega, \mu) = \psi_4(u\omega, (1-u)\omega, \mu), \quad \tilde{\psi}_4(\omega, \mu) = \omega \phi_4(\omega, \mu). \quad (152)$$

## References

- [1] T. Mannel and Y. M. Wang, JHEP **1112** (2011) 067 [arXiv:1111.1849 [hep-ph]].
- [2] T. Feldmann and M. W. Y. Yip, Phys. Rev. D **85**, 014035 (2012) [Phys. Rev. D **86**, 079901 (2012)] [arXiv:1111.1844 [hep-ph]].
- [3] W. Wang, Phys. Lett. B **708** (2014) 119 [arXiv:1112.0237 [hep-ph]].
- [4] C. S. Huang and H. G. Yan, Phys. Rev. D **59** (1999) 114022 [Phys. Rev. D **61** (2000) 039901] [hep-ph/9811303].
- [5] C. H. Chen and C. Q. Geng, Phys. Rev. D **64** (2001) 074001 [hep-ph/0106193].
- [6] P. Böer, T. Feldmann and D. van Dyk, JHEP **1501** (2015) 155 [arXiv:1410.2115 [hep-ph]].
- [7] A. Khodjamirian, T. Mannel and N. Offen, Phys. Lett. B **620** (2005) 52 [hep-ph/0504091].
- [8] A. Khodjamirian, T. Mannel and N. Offen, Phys. Rev. D **75** (2007) 054013 [hep-ph/0611193].
- [9] F. De Fazio, T. Feldmann and T. Hurth, Nucl. Phys. B **733** (2006) 1 [Nucl. Phys. B **800** (2008) 405] [hep-ph/0504088].

- [10] F. De Fazio, T. Feldmann and T. Hurth, JHEP **0802** (2008) 031 [arXiv:0711.3999 [hep-ph]].
- [11] M. Beneke, T. Feldmann and D. Seidel, Nucl. Phys. B **612** (2001) 25 [hep-ph/0106067].
- [12] Y. M. Wang and Y. L. Shen, Nucl. Phys. B **898** (2015) 563 [arXiv:1506.00667 [hep-ph]].
- [13] M. Beneke and V. A. Smirnov, Nucl. Phys. B **522** (1998) 321 [hep-ph/9711391].
- [14] P. Ball, V. M. Braun and E. Gardi, Phys. Lett. B **665** (2008) 197 [arXiv:0804.2424 [hep-ph]].
- [15] Y. M. Wang, Y. L. Shen and C. D. Lü, Phys. Rev. D **80** (2009) 074012 [arXiv:0907.4008 [hep-ph]].
- [16] P. Guo, H. W. Ke, X. Q. Li, C. D. Lü and Y. M. Wang, Phys. Rev. D **75** (2007) 054017 [hep-ph/0501058].
- [17] C. D. Lü, Y. M. Wang, H. Zou, A. Ali and G. Kramer, Phys. Rev. D **80** (2009) 034011 [arXiv:0906.1479 [hep-ph]].
- [18] G. Bell, T. Feldmann, Y. M. Wang and M. W. Y. Yip, JHEP **1311** (2013) 191 [arXiv:1308.6114 [hep-ph]].
- [19] V. M. Braun, S. E. Derkachov and A. N. Manashov, Phys. Lett. B **738** (2014) 334 [arXiv:1406.0664 [hep-ph]].
- [20] M. Knodlseder and N. Offen, JHEP **1110** (2011) 069 [arXiv:1105.4569 [hep-ph]].
- [21] W. Detmold, C.-J. D. Lin, S. Meinel and M. Wingate, Phys. Rev. D **87** (2013) 074502 [arXiv:1212.4827 [hep-lat]].
- [22] Y. M. Wang, Y. Li and C. D. Lü, Eur. Phys. J. C **59** (2009) 861 [arXiv:0804.0648 [hep-ph]].
- [23] Y. L. Liu, C. Y. Cui and M. Q. Huang, Eur. Phys. J. C **74** (2014) 3041 [arXiv:1407.4889 [hep-ph]].
- [24] V. L. Chernyak and I. R. Zhitnitsky, Nucl. Phys. B **246** (1984) 52.
- [25] T. M. Aliev, K. Azizi and M. Savci, Phys. Rev. D **81** (2010) 056006 [arXiv:1001.0227 [hep-ph]].
- [26] L. F. Gan, Y. L. Liu, W. B. Chen and M. Q. Huang, Commun. Theor. Phys. **58** (2012) 872 [arXiv:1212.4671 [hep-ph]].
- [27] V. M. Braun, A. Lenz and M. Wittmann, Phys. Rev. D **73** (2006) 094019 [hep-ph/0604050].

- [28] X. G. He, T. Li, X. Q. Li and Y. M. Wang, Phys. Rev. D **74** (2006) 034026 [hep-ph/0606025].
- [29] A. Khodjamirian, C. Klein, T. Mannel and Y.-M. Wang, JHEP **1109** (2011) 106 [arXiv:1108.2971 [hep-ph]].
- [30] V. L. Chernyak, A. A. Ogloblin and I. R. Zhitnitsky, Z. Phys. C **42** (1989) 569 [Yad. Fiz. **48** (1988) 1410] [Sov. J. Nucl. Phys. **48** (1988) 896].
- [31] V. Braun, R. J. Fries, N. Mahnke and E. Stein, Nucl. Phys. B **589** (2000) 381 [Nucl. Phys. B **607** (2001) 433] [hep-ph/0007279].
- [32] S. Wandzura and F. Wilczek, Phys. Lett. B **72** (1977) 195.
- [33] G. Bonneau, Nucl. Phys. B **167** (1980) 261.
- [34] G. Bonneau, Nucl. Phys. B **171** (1980) 477.
- [35] C. W. Bauer, S. Fleming, D. Pirjol and I. W. Stewart, Phys. Rev. D **63** (2001) 114020 [hep-ph/0011336].
- [36] M. Beneke, Y. Kiyo and D. S. Yang, Nucl. Phys. B **692** (2004) 232 [hep-ph/0402241].
- [37] G. Bell, M. Beneke, T. Huber and X. Q. Li, Nucl. Phys. B **843** (2011) 143 [arXiv:1007.3758 [hep-ph]].
- [38] M. Beneke and J. Rohrwild, Eur. Phys. J. C **71** (2011) 1818 [arXiv:1110.3228 [hep-ph]].
- [39] J. Y. Chiu, A. Jain, D. Neill and I. Z. Rothstein, JHEP **1205** (2012) 084 [arXiv:1202.0814 [hep-ph]].
- [40] H. N. Li, Y. L. Shen and Y. M. Wang, JHEP **1302** (2013) 008 [arXiv:1210.2978 [hep-ph]].
- [41] H. N. Li, Y. L. Shen and Y. M. Wang, JHEP **1401** (2014) 004 [arXiv:1310.3672 [hep-ph]].
- [42] Y. L. Shen and Y. M. Wang, EPJ Web Conf. **80** (2014) 00047 [arXiv:1409.1048 [hep-ph]].
- [43] R. Aaij *et al.* [LHCb Collaboration], Phys. Lett. B **725** (2013) 25 [arXiv:1306.2577 [hep-ex]].
- [44] R. Aaij *et al.* [LHCb Collaboration], JHEP **1506** (2015) 115 [arXiv:1503.07138 [hep-ex]].
- [45] T. Aaltonen *et al.* [CDF Collaboration], Phys. Rev. Lett. **107** (2011) 201802 [arXiv:1107.3753 [hep-ex]].
- [46] M. Beneke and T. Feldmann, Nucl. Phys. B **592** (2001) 3 [hep-ph/0008255].
- [47] S. Groote, J. G. Korner and O. I. Yakovlev, Phys. Rev. D **56** (1997) 3943 [hep-ph/9705447].

- [48] Y. L. Liu and M. Q. Huang, Nucl. Phys. A **821** (2009) 80 [arXiv:0811.1812 [hep-ph]].
- [49] M. Beneke, A. Maier, J. Piclum and T. Rauh, Nucl. Phys. B **891** (2015) 42 [arXiv:1411.3132 [hep-ph]].
- [50] A. Khodjamirian, T. Mannel, N. Offen and Y.-M. Wang, Phys. Rev. D **83** (2011) 094031 [arXiv:1103.2655 [hep-ph]].
- [51] A. Khodjamirian, T. Mannel, A. A. Pivovarov and Y.-M. Wang, JHEP **1009** (2010) 089 [arXiv:1006.4945 [hep-ph]].
- [52] H. n. Li, Y. L. Shen and Y. M. Wang, Phys. Rev. D **85** (2012) 074004 [arXiv:1201.5066 [hep-ph]].
- [53] W. F. Wang and Z. J. Xiao, Phys. Rev. D **86** (2012) 114025 [arXiv:1207.0265 [hep-ph]].
- [54] S. Groote, J. G. Korner and O. I. Yakovlev, Phys. Rev. D **55** (1997) 3016 [hep-ph/9609469].
- [55] C. Bourrely, I. Caprini and L. Lellouch, Phys. Rev. D **79** (2009) 013008 [Phys. Rev. D **82** (2010) 099902] [arXiv:0807.2722 [hep-ph]].
- [56] W. Detmold, C. Lehner and S. Meinel, Phys. Rev. D **92** (2015) 3, 034503 [arXiv:1503.01421 [hep-lat]].
- [57] K. A. Olive *et al.* [Particle Data Group Collaboration], Chin. Phys. C **38** (2014) 090001.
- [58] W. A. Bardeen, E. J. Eichten and C. T. Hill, Phys. Rev. D **68** (2003) 054024 [hep-ph/0305049].
- [59] A. V. Manohar and M. B. Wise, Camb. Monogr. Part. Phys. Nucl. Phys. Cosmol. **10** (2000) 1.
- [60] T. Mannel and S. Recksiegel, J. Phys. G **24** (1998) 979 [hep-ph/9701399].
- [61] Y. M. Wang, J. Phys. Conf. Ser. **556** (2014) 1, 012050.
- [62] H. Miyake, S. Kim and F. Ukegawa [CDF Collaboration], Public Note 10894, (<http://www-cdf.fnal.gov/physics/new/bottom/bottom.html>).
- [63] R. Aaij *et al.* [LHCb Collaboration], Nature Phys. **11** (2015) 743 [arXiv:1504.01568 [hep-ex]].